Manuscript prepared for Atmos. Meas. Tech. Discuss.
with version 2015/04/24 7.83 Copernicus papers of the LaTeX class copernicus.cls.
Date: 10 July 2015

Three years of semi-continuous greenhouse gas measurements at Puy de Dôme station (Central France)

M. Lopez[1,*], M. Schmidt[1,], M. Ramonet[1], J.-L. Bonne[1], A. Colomb[2], V. Kazan[1], P. Laj[3], and J.-M. Pichon[2,4]**

[1]Laboratoire des Sciences du Climat et de l'Environnement (LSCE – UMR8212), Unité mixte CEA-CNRS-UVSQ, 91191 Gif-sur-Yvette, France
[2]Laboratoire de Météorologie Physique, Université Blaise Pascal, Clermont-Université, CNRS, UMR 6016, 63171, Aubière, France
[3]Université Grenoble Alpes, CNRS, Laboratoire de Glaciologie et Géophysique de l'Environnement (LGGE – UMR 5183), 38402 Saint-Martin d'Hères, France
[4]Observatoire de Physique du Globe de Clermont-Ferrand, Université Blaise Pascal, Clermont Université, CNRS, UMS 833, 63171, Aubière, France
[*]now at: Environment Canada, Climate Research Division, Toronto, Ontario, Canada
[**]now at: Institut für Umweltphysik, University of Heidelberg, Heidelberg, Germany

Correspondence to: M. Ramonet (michel.ramonet@lsce.ipsl.fr)

Abstract

Three years of greenhouse gas measurements, obtained using a gas chromatograph (GC) system located at the Puy de Dôme station at 1465 m a.s.l. in Central France are presented. The GC system was installed in 2010 at Puy de Dôme and was designed for automatic and accurate semi-continuous measurements of atmospheric carbon dioxide, methane, nitrous oxide and sulfur hexafluoride mole fractions. We present in detail the instrumental set up and the calibration strategy, which together allow the GC to reach repeatabilities of 0.1 µmol mol^{-1}, 1.2 nmol mol^{-1}, 0.3 nmol mol^{-1} and 0.06 pmol mol^{-1} for CO_2, CH_4, N_2O and SF_6, respectively. ~~Comparisons of the atmospheric time series with those obtained using other instruments show that the GC system meets the World Meteorological Organization recommendations.~~ The analysis of the three-year atmospheric time series revealed how the planetary boundary layer height drives the mole fractions observed at a mountain site such as Puy de Dôme where air masses alternate between the planetary boundary layer and the free troposphere.

Accurate long-lived greenhouse gas measurements collocated with ^{222}Rn measurements as an atmospheric tracer, allowed us to determine the CO_2, CH_4 and N_2O emissions in the catchment area of the station. The derived CO_2 surface flux revealed a clear seasonal cycle with net uptake by plant assimilation in the spring and net emission caused by the biosphere and burning of fossil fuel during the remainder of the year. We calculated a mean annual CO_2 flux of $1150 \pm 600\,t(CO_2)\,km^{-2}$. The derived CH_4 and N_2O emissions in the station catchment area were $6.2 \pm 3.5\,t(CH_4)\,km^{-2}\,yr^{-1}$ and $1.5 \pm 0.9\,t(N_2O)\,km^{-2}\,yr^{-1}$, respectively. Our derived annual CH_4 flux is in agreement with the national French inventory, whereas our derived N_2O flux is five times larger than the same inventory.

1 Introduction

The release of anthropogenic greenhouse gases (GHGs) in the atmosphere leads to a modification of their natural cycles and a strong increase in atmospheric radiative forcing (Myhre

et al., 2013). The Intergovernmental Panel on Climate Change (IPCC) reported that the global average temperature increased by 0.89 °C between 1901 and 2012 (Hartmann et al., 2013) and will continue to increase during the 21st century (Collins et al., 2013). To limit the global temperature rise, most industrialized countries signed the "United Nations Framework Convention on Climate Change" (UNFCCC) treaty in 1992 to stabilize their GHG emissions between 1990 and 2000 **and entered into force in 1994**. This convention was enhanced by the Kyoto Protocol, which was signed in 1997 and was ratified by 182 countries. The countries engaged in the Kyoto protocol aimed to reduce their national emissions of the ~~six~~ main long-lived GHGs by 5.2 % between 2008 and 2012, compared to emission levels of 1990: carbon dioxide (CO_2), methane (CH_4), nitrous oxide (N_2O), sulfur hexafluoride (SF_6), hydrofluorocarbons (HFCs) and perfluorocarbons (PFCs). The European Union (EU) committed to reduce its GHG emissions by 8 % for the same period. In addition, the EU aims to reduce its total GHG emissions by 20 % in 2020, relative to emissions in 1990. Despite this commitment, it is extremely difficult to validate the surface GHG fluxes at the country scale using a reliable, transparent method.

Currently, countries report their respective GHG emissions to the UNFCCC on an annual basis. These national emission inventories are based on bottom-up methods and the reliability of these national inventories strongly depends on the uncertainty attributed to each emission factor. To improve and validate the bottom-up methods, it is crucial to better characterize the biogeochemical cycles of the different GHGs, particularly as national inventories report only anthropogenic emissions to the UNFCCC. Therefore, it is important to develop new tools to quantify natural sources emissions and to provide an independent verification of the emission inventories reported to the UNFCCC.

Different methods based on atmospheric measurements can be used to estimate GHG emissions at local to regional scales. **Some of** these approaches couple atmospheric GHG measurements with measurements of associated atmospheric tracers of air masses, including radon-222 (Biraud et al., 2000; Schmidt et al., 2001), sulfur hexafluoride (Maiss et al., 1996) or isotopes like radiocarbon in CO_2 (Levin and Karsten, 2007; Lopez et al., 2013). A major advantage of this "multigas" approach is that it avoids the use of complex

chemistry-transport models; the tracers that are used are subject to the same atmospheric transport mechanisms as the GHGs. Nevertheless, an accurate assessment of the respective measurement station footprint is required to allocate the estimated surface fluxes to a specific region (Gloor et al., 2001).

The first atmospheric CO_2 continuous measurements started in the 1950s at Mauna Loa observatory using a Non Dispersive Infra Red (NDIR) analyzer with a repeatability better than 0.1 µmol mol^{-1} (Keeling et al., 1976). Atmospheric CH_4 monitoring began in the late 1970s using gas chromatograph (GC) systems equipped with a flame ionization detector (FID) and a nickel catalyst to enable simultaneous CO_2 mole fraction detection (Rasmussen and Khalil, 1981). The repeatabilities were approximately 10 nmol mol^{-1} for CH_4 measurements and 0.7 µmol mol^{-1} for CO_2 measurements. Coupling an electron capture detector (ECD) to a GC system enabled the detection of N_2O and SF_6 atmospheric mole fractions with repeatabilities of approximately 1.0 nmol mol^{-1} and 0.1 pmol mol^{-1}, respectively (Weiss, 1981; Prinn et al., 1990; Maiss et al., 1996). Subsequently, the use of two detectors (FID and ECD) has permitted the use of GC to analyze CO_2, CH_4, N_2O and SF_6 atmospheric mole fractions simultaneously and on a semi-continuous basis. Since the 1980s, atmospheric monitoring stations that are part of the Global Atmosphere Watch (GAW), have been gradually equipped with GC systems and NDIR analyzers. The GC system technologies described above have continuously evolved to reach repeatabilities better than 0.1 µmol mol^{-1} for CO_2, 2.0 nmol mol^{-1} for CH_4, 0.3 nmol mol^{-1} for N_2O and 0.1 pmol mol^{-1} for SF_6, as shown by van der Laan et al. (2009b), Thompson et al. (2009) or Popa et al. (2010).

New types of accurate instruments for CO_2, CH_4 and N_2O atmospheric measurements have recently become commercially available. These instruments are based on optical technologies, including cavity ring down spectroscopy (CRDS), Fourier transform infra red spectrometry (FTIR) or off-axis integrated cavity output spectroscopy (OA-ICOS) ~~can be cited~~. These recent technologies are promising for atmospheric monitoring as they offer real continuous measurements (acquisition frequency on the order of 1 Hertz), require low maintenance and achieve equivalent or superior repeatability compared to GC systems (Yver

Kwok et al., 2015; Hammer et al., 2013a). Analyzers based on the CRDS technology are generally used for CO_2 and CH_4 atmospheric measurements, OA-ICOS technology is used for N_2O measurements, and FTIR technology is designed to simultaneously measure CO_2, CH_4 and N_2O. These new types of instruments are also more easily transportable, and Hammer et al. (2013b) have demonstrated their feasibility as "traveling" instruments. They could thus be used for comparisons and quality control purposes to ensure data compatibility through a monitoring network.

Regardless of the benefits listed above, these optical technologies cannot be used to measure yet atmospheric SF_6 mole fractions, which is ~~the fourth anthropogenic GHG in terms of radiative forcing~~ **an extremely stable GHG having a global warming potential of 23,900** (Forster et al., 2007). In addition, most of these new technologies need to be continuously flushed, which makes it difficult to analyze flasks, in contrast to the GC systems, which employ discrete samples and can analyze four or five species simultaneously (van der Laan et al., 2009b). Studies of optical technologies are still progressing, and as noted above, these new technologies are very promising, particularly for a dense monitoring network, such as the European infrastructure ICOS (Integrated Carbon Observation System), which is dedicated to high precision monitoring of greenhouse gases over Europe. The CRDS technology is slowly replacing the GC systems or NDIR analyzers for CO_2 and CH_4 monitoring in many stations, but GC is still the reference instrument for N_2O and SF_6 measurements (see WMO-GAW, 2013). Consequently, we installed a GC system in 2010 at the mountain station of Puy de Dôme (France) to monitor with high precision the long-term atmospheric trend of the main four long-lived greenhouse gases.

This paper focuses on three years of ambient air measurements of CO_2, CH_4, N_2O and SF_6 obtained using a GC system at the Puy de Dôme station (2010 to 2013). After a short description of the station, the detailed setup of the GC as well as the calibration strategy are addressed. A paragraph is dedicated to data quality control and atmospheric measurement comparisons~~, which demonstrated that~~ showing in which conditions our measurement system reaches the WMO recommendations (WMO-GAW, 2013). In the last part, we present and analyze our three-year time series of ambient air measurements. Finally, we demon-

strate that these time series can be used to estimate the monthly regional fluxes ~~densities~~ of CO_2, CH_4 and N_2O in the catchment area of Puy de Dôme station, using the radon-222 as an atmospheric tracer.

2 The Puy de Dôme station

2.1 Site description

Puy de Dôme station (45°46′19″ N, 2°57′57″ E) is located at the top of the Puy de Dôme volcano, 1465 m a.s.l., in the Auvergne region in the center of France. This station is managed by the Laboratoire de Météorologie Physique (LaMP) and is part of the Observatoire de Physique du Globe de Clermont-Ferrand (OPGC) located at Clermont-Ferrand, France. According to the French national institute of statistic and economic studies (INSEE – http://www.insee.fr), **the ground cover of Auvergne region (26,013 km^{-2}) consists mainly of meadows (36.4 %), forests (33.4 %) and arable land (17.6 %), Puy de Dôme station being located in the center of this region.** ~~Puy de Dôme is surrounded by meadows (36.4 %), forests (33.4 %) and arable land (17.6 %)~~. The major anthropogenic GHG sources are on the east of the station where the town of Clermont-Ferrand is located 10 km east of the Puy de Dôme station at an altitude of 396 m a.s.l. Clermont-Ferrand is the largest town in the region, with approximately 150 000 inhabitants.

The CITEPA (Centre Interprofessionnel Technique d'Etudes de la Pollution Amosphérique) reports the French national GHG emissions to the UNFCCC but has also provided a regional inventory of Auvergne for the year 2007 (CITEPA, 2010). According to the CITEPA, the anthropogenic CO_2 emissions in the Auvergne region are mainly attribuable to road transport, residential and industrial sectors, which represent respectively 45, 25 and 21 % of the total anthropogenic CO_2 emissions of the region. The agricultural sector is responsible for 90 % of total anthropogenic CH_4 emissions and 97 % of total anthropogenic N_2O emissions in the region. Ninety percent of the SF_6 emissions are related to the energy transformation sector.

A military base and a telecommunication center are located 20 m northwest of the station, also on the top of the volcano. These facilities consist of a main building with a height of 20 m and a telecommunication antenna with a height of 89 m. Since 2010, the only access road to the station has been closed to the public and has been replaced by a cog train.

The atmospheric research station hosts different analyzers for long-term atmospheric measurements of GHG, CO, O_3, aerosols, radon-222, clouds microphysics and radionuclide. The station has international labeling EMEP (European Monitoring and Evaluation Programme), GAW, and is part of the European ACTRIS (Aerosol **particles**, Clouds, and Trace gases Research Infrastructure) and ICOS measurement networks.

2.2 Atmospheric conditions at the Puy de Dôme station

Meteorological parameters are monitored at the station, including wind speed, wind direction, temperature, relative humidity and atmospheric pressure. A wind shadow area between 300 and 360° is clearly observed in the wind direction due to the building and the telecommunication antenna of the military base, which both induce local turbulences. The planetary boundary layer (PBL) height, wind speed and wind direction were extracted from the European Center for Medium-range Weather Forecasts (ECMWF, 2012; Seidel et al., 2012) at a three-hour time resolution for the years 2010 to 2012. The grid cell used for the extraction had an area of $15\,\mathrm{km} \times 15\,\mathrm{km}$ and was centered at 45°45′ N, 3°00′ E at an altitude of 575 m a.s.l. In this study, the wind direction from ECMWF was used as the reference because the wind direction provided by the meteorological sensor is influenced by the local turbulences **caused by the telecommunication antenna located on the military base**. The average difference in wind speed between the meteorological station and the ECMWF data was $3.4 \pm 4.3\,\mathrm{m\,s^{-1}}$, the wind speed measured by the sensor was higher because the sensor is located at a higher elevation than the grid cell used for the ECMWF extraction (1465 m a.s.l. compared to 575 m a.s.l.). Therefore the wind speed from the meteorological sensor was used to correct the ECMWF data. The PBL height and the wind direction from ECMWF were interpolated using a linear regression fit to obtain a one-hour time resolution.

~~Regarding meteorological parameters,~~ The Puy de Dôme station is primarily influenced by winds from a south-west direction (48.2 % of the time) with a mean wind speed of 8.4 $\mathrm{m\,s^{-1}}$. The wind blows from Clermont-Ferrand sector (45–135°) only 7.7 % of the time, with a mean speed of 4.2 $\mathrm{m\,s^{-1}}$. The PBL height analysis revealed that the Puy de Dôme station is in the free troposphere during more than 70 % of the time and up to 81 % during winter time.

Backtrajectories were calculated using the Lagrangian dispersion model Flexpart version 8.2.3, based on ECMWF ERA-Interim data at a horizontal resolution of $1^\circ \times 1^\circ$, with 60 vertical levels and 3 h temporal resolution. ~~Air masses were released~~**Eight particles were released every 15 min (96 particles every 3 h)** in a 3-D box centered around the Puy de Dôme station (from lower left corner 45.76° N, 2.95° E to upper right corner 45.78° N, 2.97° E, between 1400 and 1500 m a.s.l.) with a lifetime of 3 days. ~~Eight particles were released every 15 min (96 particles every 3 h)~~. This simulation was performed for particles arriving at the station between 1 January 2010 and 31 December 2012. The footprints were computed on a $1^\circ \times 1^\circ$ horizontal grid, following the method described by Lin et al. (2003), taking into account the planetary boundary layer height at each particle location. We considered that a particle is influenced by surface emissions from one grid cell when its elevation is under the PBL height and that its influence is inversely proportional to the PBL height. The maps presented on Fig. 1 respectively show the footprints for air masses arriving at the station between 14:00 and 16:00 UTC when the PBL is usually well developed (Fig. 1a), and between 22:00 and 06:00 UTC when the PBL is below 1400 m and the station is within the free troposphere (Fig. 1b). The grid cells influence is represented as a relative influence compared to the maximum value (in percent). On both maps, the station is located within the black grid cell. Boulon et al. (2011) showed that 87 % of air masses reaching the station are from the west by analysing backtrajectories from HYSPLIT over 437 days at Puy de Dôme (i.e., from Atlantic and continental Western Europe areas). A statistical analysis of backtrajectories over four years conducted by Venzac et al. (2009) demonstrated that winter air masses reaching Puy de Dôme travel over longer distances from the west than summer air masses.

3 Instrumental setup

The GHG observations at Puy de Dôme started in 2000 with continuous CO_2 measurements using a non-dispersive infra-red (NDIR) spectrometer. Since 2001, a pair of flasks has been sampled once a week by the LaMP team and analyzed by GC for CO_2, CH_4, N_2O and SF_6 mole fractions and by a mass spectrometer for $\delta^{13}C$ and $\delta^{18}O$ in CO_2 at the LSCE in Gif-sur-Yvette, France. In 2010, a GC system for semi-continuous measurements of CO_2, CH_4, N_2O and SF_6 was installed at the station. In 2011, the NDIR spectrometer was replaced by a CRDS for continuous CO_2 and CH_4 measurements. Since 2002, the station has also been equipped with a radon-222 (^{222}Rn) analyzer based on the active deposit method. These instruments are housed in a regulated temperature room, and the inlet lines are located on the roof of the station, 10 m a.g.l. This section focuses on the setup of the GC installed at the Puy de Dôme station in July 2010.

3.1 Description of the GC system

The GC system installed at the Puy de Dôme station is a commercial HP-6890N from Agilent, that was modified and optimized at the LSCE for automatic and semi-continuous atmospheric measurements of CO_2, CH_4, N_2O and SF_6 mole fractions in dry ambient air (Lopez, 2012). Similar instrument configurations are installed at the Gif-sur-Yvette and Trainou stations in northern France (Lopez et al., 2012; Schmidt et al., 2014).

The ambient air is pumped from the roof of the station (pump KNF: PMF 1433-811) through 10 m long decabon tube with an outside diameter of $1/2$ in (~ 1.27 cm). Three filters (140, 40 and 7 µm TF series from Swagelok) are placed in series to protect the pump and the analysis system from dust and aerosols. After passing the pump, the ambient air is pressurized and dried in two steps. First, the air passes through a commercial decanting bowl (40 mL volume) placed in a refrigerator set at 5 °C for preliminary drying. The water accumulated in the decanting bowl is flushed out every six hours for 10 s by opening a solenoid valve. In a second step, the ambient air passes through a glass trap that is maintained in an ethanol bath at -55 °C by a cryocooler (Thermo Neslab CC-65)~~to remove the~~

~~remaining water vapor.~~ **The dew point of the air going in the instrument is $-50\,^{\circ}\mathrm{C}$**. The glass trap is changed during the weekly maintenance of the station. An electronic box is used to regulate the refrigerator temperature and to switch the solenoid valve of the decanting bowl. This box also records the temperatures of the fridge, the ethanol bath and the room. In case of power failure, the entire GC system is connected to an uninterruptible power supply (UPS), that allows the system to run for a few hours.

The GC system consists of an injection part, a separation part and a detection part. These different parts are indicated by different colors in Fig. 2. For analysis, an air sample is first filled into the two sample loops. The sample is then pushed by different carrier gases to the chromatographic columns, where the species are separated. Finally, CO_2 (via a nickel catalyst) and CH_4 are detected by a FID. A micro electron capture detector (μECD) is used to detect N_2O and SF_6. One injection and analysis requires 5.4 min.

3.1.1 Sample analysis

The injection part (framed by green in Fig. 2) consists of an 8-port microelectronic valve ♯7 (model DC8WE from Valco vici, Switzerland) that enables the selection of the samples to be analyzed (ambient air or gas cylinders). The selected sample is injected into the system via an electronic pressure control (EPC-Aux5) through two sample loops **located in the room**. The sample loops are placed in series on two 6-port 2-way Valco valves (♯1a and ♯1b). The sample loop for CO_2 and CH_4 analysis has a volume of 15 mL (sample loop on the ♯1a valve) and the one for N_2O and SF_6 analysis has a volume of 10 mL (sample loop on the ♯1b valve). The sample loops are flushed with sample gas for 0.75 min at a flow rate of 180 mL min^{-1} (corresponding to 2.5 psi pressure on Aux5). Before injection, the two sample loops are equilibrated at temperature and atmospheric pressure for 0.5 min by setting Aux5 to 0 psi. After equilibration, the samples are injected into the columns with the respective carrier gases by switching valve ♯1a and ♯1b. The carrier gas used for the FID is N_2 (purity > 99,9999 %), whereas a mixture of argon/methane (95/5 %, ECD quality) is used as the carrier gas for the μECD. A purifying cartridge (Aeronex) is placed after each carrier gas cylinder.

The columns used to separate the different molecules are placed in an oven regulated at 80 °C (see the portion framed by yellow in Fig. 2). A Hayesep-Q ($12' \times 3/16''$SS, mesh 80/100) analytical column is used for CO_2 and CH_4 separation. For N_2O and SF_6 separation, a pre-column Hayesep-Q ($4' \times 3/16''$SS, mesh 80/100) and an analytical column Hayesep-Q ($6' \times 3/16''$SS, mesh 80/100) are used. The pre-column is back-flushed between 0 and 0.75 min and between 3.7 and 5.4 min with a 100 mL min^{-1} flow rate of the carrier gas to eliminate heavy electrophilic molecules from the system to avoid an eventual pollution of the analytical column, which might induce an increase in the μECD baseline. Between 0.75 and 3.7 min, the N_2O and SF_6 molecules are transported first through the pre-column and then in the analytical column, where separation occurs. The analytical column is directly connected to the μECD. The N_2O and SF_6 retention times are 4.3 and 4.8 min, respectively.

The CH_4 and CO_2 molecules are detected by an FID **and a Ni-catalyst, which reduces CO_2 to CH_4**. Methane molecules elutes after 2.7 min and are injected directly into the detector for analysis. Once the CH_4 molecules are released from the analytical column, the Valco valve ♯4 is switched to connect the nickel catalyst to allow CO_2 molecules to be reduced to CH_4 to enable CO_2 detection by the FID. The retention time of CO_2 is 3.5 min. The FID temperature is controlled at 300 °C, and the flame is fed with a 65 mL min^{-1} flow rate of hydrogen (provided by a NM-H2 hydrogen generator from F-DBS) and a 400 mL min^{-1} flow rate of zero air (provided by a combination of a compressor from June-Air and a 75-82 air zero generator from Parker-Balston). Hydrogen is also used for CO_2 ~~catalysis by the nickel catalyst~~**reduction over the Ni catalyst**. The typical efficiency of the catalyst is 97 % in the CO_2 atmospheric mole fractions range.

We used the numbering system used by Agilent for naming each of the valves and the EPCs.

Figure 3 shows the typical chromatograms obtain by the two detectors used in the GC system. The top panel presents the FID's response in pA. The spike observed between the CH_4 peak and the CO_2 peak in the zoomed panel is caused by the switching of valve ♯4. The bottom panel of Fig. 3 presents the µECD's response in Hz. The

first large peak observed at approximately 2.7 min is the O_2 peak which is following by the N_2O peak and finally by the SF_6 peak.

3.1.2 Analysis management

Data acquisition, valve switching and temperature regulation of the GC system are entirely processed by Chemstation software (version A.10.02, Agilent). This software allows the control of the GC system parameters through the so-called "methods". A typical method is configured to perform the following:

- control the temperature of the detectors, the catalyst and the oven;
- regulate the flow of the sample (via Aux5), the carrier gases (via Aux3 and Aux4), H_2 and zero air, all via five distinct EPCs;
- schedule the switching of the four 6-port 2-way Valco valves, controlled via the internal events output GC connector;
- choose the position of the 8-port microelectronic Valco valve, controlled via the external events output GC connector;
- integrate the results of the analysis (via the chromatograms).

A typical method is presented in Table 1 and corresponds to one analysis of a chosen sample. Table 2 summarizes the GC system setup used between 2010 and 2013. ~~A sequence is based on several successive methods. The arrangement of the methods in a sequence enables the automatic selection of the order of samples measurements (ambient air, calibration or quality control cylinders) over several days.~~ **A sequence is designed for lasting three days by sequential arrangement of methods which enable the automatic selection of ambient air and calibration gas measurement. The created sequence is run in a loop mode.**

The FID and μECD signals (chromatograms) are expressed in pA and Hz, respectively. The peak integrations (area and height) of the different chromatograms are automatically

computed by the Chemstation software at the end of each method and the integration results are stored in ".txt" files. The repeatability of our GC system (see Sect. 3.3) is improved when the peak areas for CO_2, CH_4 and N_2O and the peak heights for SF_6 are used. Once a day, the integration results are transferred to and stored in the LSCE database via ftp, and the mole fractions of the analyzed samples are automatically calculated. Three to five times each week, ~~the GC system performance is controlled via a graphical application by a trained operator~~ **a trained operator evaluates the performances of the GC through a dedicated graphical application enabling to draw graphics of the instrument parameters** (see Sect. 3.3). Based on these graphics, flags are manually assigned to the data.

3.1.3 Calibration strategy

The GC system is calibrated using a two-point calibration strategy. Two working standards containing a known amount of CO_2, CH_4, N_2O and SF_6 in synthetic air (matrix of N_2, O_2 and Ar) are used. The mole fractions of the trace gases in the two working standards are selected to bracket the typical ambient air mole fractions observed at the Puy de Dôme station and are referred to as working standard high (WH) and working standard low (WL). These gas mixtures are used to fill 40 L aluminum cylinders (Luxfer) to 200 bar by Deuste Steininger (Mühlhausen, Germany). All working standards are calibrated at LSCE against the laboratory standard scale of the World Meteorological Organization (WMO scale) provided by the Central Calibration Laboratories (CCL) of the National Oceanic and Atmospheric Administration (NOAA). The calibration scales currently used are WMO-X2007, NOAA-04, NOAA-2006A and NOAA-2006 for CO_2, CH_4, N_2O and SF_6, respectively: Zhao and Tans (2006); Hall et al. (2007); Dlugokencky et al. (2005).

The response function of μECD for N_2O analysis is non-linear**, especially in the range below and above the tropospheric values** (see Schmidt et al., 2001; van der Laan et al., 2009b; Lopez et al., 2012). The non-linearity of our μECD was tested by analyzing five cylinders calibrated by the CCL on the NOAA-2006A scale and with N_2O mole fractions between 302.00 and 338.04 nmol mol^{-1}. **In this small mole fraction range, which is important for our measurements, a two point calibration describes sufficient the response**

function of our μECD. ~~We have determined that a linear fit is sufficient to account for the non-linearity of our μECD. The two-point calibration strategy~~ **It** compares very well with an exponential fit through five cylinders, with an average difference of $0.01 \pm 0.13\,\mathrm{nmol\,mol^{-1}}$. This result confirms that a two-point calibration strategy is well adapted to correct for the μECD non-linearity in atmospheric mole fraction ranges. Similar tests demonstrated that the FID response is linear in the atmospheric mole fractions range for CO_2 and CH_4 measurements.

The two working standards (WH and WL) are analyzed every 30 min to correct for atmospheric (temperature and pressure) changes as well as instrumental drifts, enabling the analysis of five samples between each calibration. The lifetime of our standards is approximately three years using this calibration strategy. To limit the risk of drift, each working standard must be replaced before reaching 30 bar pressure. At the end of their use at the station, all working standards are recalibrated at LSCE to verify their stability over their lifetimes. At Puy de Dôme station, the first set of working standards was replaced on 25 April 2013. Re-analysis of the standards at LSCE revealed mean differences (2010–2013) of $-0.11\,\mu\mathrm{mol\,mol^{-1}}$, -0.03, $-0.1\,\mathrm{nmol\,mol^{-1}}$ and $0.0\,\mathrm{pmol\,mol^{-1}}$ for CO_2, CH_4, N_2O and SF_6, respectively. **The observed differences are not statistically significant but for CO_2. The calibration cylinders have respectively drifted by 0.08 and 0.15 $\mu\mathrm{mol\,mol^{-1}}$ over their lifetime for CO_2. The CO_2 data presented in this paper are not corrected for the observed drift on the order of 0.03 $\mathrm{mol\,mol^{-1}\,yr^{-1}}$.** The first measurement period (July 2010 to 24 April 2013) is called "period A" in this paper, and the second measurement period (after the change of the working standards) is called "period B" (from 25 April 2013 to 30 June 2013). The mole fractions of the working standards used at Puy de Dôme are presented in Table 3.

3.2 Other instrumentation

3.2.1 Flask sampling unit

Since 2002, a flask sampling unit has been installed at the Puy de Dôme station for weekly sampling. It consists of a pump that pressurizes two 1 L glass flasks in series to 1 bar relative pressure. They are flushed for 15 min with dry ambient air prior to pressurization. Ambient air is dried in a distinct cooling trap maintained in the same ethanol bath as the GC trap (see Sect 3.1). The flasks are then shipped and analyzed at LSCE for CO_2, CH_4, N_2O and SF_6 by a GC system and for CO_2 isotopic composition (^{13}C and ^{18}O) by a Finnigan MAT-252 isotope mass spectrometer. The calibrations for trace gas analysis are performed in the same manner as presented in Sect. 3.1.3, and the results are stored in the same database.

3.2.2 Radon-222 measurement system

Radon-222 (^{222}Rn) is a radioactive noble gas ($T_{1/2} = 3.8$ days) and is part of the radioactive decay chain of uranium-238. Uranium-238 in the earth's crust results in the emission of ^{222}Rn by the earth's surface. Atmospheric radon-222 activity has been monitored at Puy de Dôme station since 2002. The analyzer is based on the active deposit method, which consists of alpha decay counting of ^{222}Rn's solid short-lived daughters: ^{218}Po, ^{214}Pb and ^{214}Bi. The measurement technique has been described in detail by Polian et al. (1986) or Biraud et al. (2000). To avoid the loss of the solid ^{222}Rn daughters, the inlet line is a 6 m long straight metal tube 35 mm in **outside** diameter. During the first years of measurements, the inlet line was frequently contaminated by room air and only measurements after October 2006 can be used. Schmidt (1999) estimated a radioactive disequilibrium (see Turner, 1964) at the Schauinsland station (Germany – 47°54′ N, 7°54′ E – 1205 m a.s.l.) of 1.15 ± 0.14. This value was independently confirmed by Xia et al. (2010). The Puy de Dôme station and the Schauinsland station are two medium-elevation mountain having the same geographical environment. They are both frequently above the continental boundary layer, especially in winter. Based on the similarities between the Puy de Dôme station and the

Schauinsland station, the measured (^{222}Rn) activity at Puy de Dôme has been corrected for the radioactive disequilibrium by using the same value (1.15 ± 0.14).

3.2.3 CO_2 continuous measurements by in situ NDIR

Continuous CO_2 measurements at Puy de Dôme began in 2000 with a NDIR gas analyzer. The instrument is an integrated system constructed around a LICOR NDIR (Li-6252 NDIR, LI-COR Inc., Nebraska, USA) analyzer optical bench. The CO_2 measurements are based on the difference in absorption of infrared radiation passing through two cells: the reference cell and the sample cell. Infrared radiation is transmitted through both cell paths, and the analyzer signal is proportional to the difference in absorption between both cells. The measurement frequency is 1 Hz, and the cell flow is typically 20 mL min^{-1} for the sampling cell, and 15 mL min^{-1} for the reference cell **which is continuously flushed with a reference gas**. The calibration strategy is based on four cylinders calibrated on the WMO-X2007 scale. The calibration is performed twice a year by analyzing each calibration cylinder 30 times for 10 min. Data are then corrected using a quadratic fit.

Ambient air is pumped from the roof to the instrument through a $3/8$ in (~ 0.95 cm) **outside diameter** decabon line. The air is dried by passing through a glass trap maintained in a cold ethanol bath (see Sect. 3.1). Ambient air is analyzed for 50 min following the analysis of the reference cylinder for 10 min**, which is passed through both cells at the same time**. The NDIR spectrometer was replaced by a CRDS analyser in April 2011.

3.2.4 CO_2 and CH_4 continuous measurements by in situ CRDS

The CRDS analyzer (Picarro G1301) was installed in April 2011. It continuously and simultaneously measures CO_2, CH_4 and H_2O atmospheric mole fractions. We use four calibration cylinders spanning the atmospheric range of 366 to 453 µmol mol^{-1} for CO_2 and 1722 to 2107 nmol mol^{-1} for CH_4. The cylinders are calibrated at the LSCE laboratory on the WMO-X2007 and NOAA-04 scales, respectively. The instrument calibration is performed automatically every 15 days by injection of the following scheme: 4 times each calibration

cylinder for 30 min, beginning with the one with the lowest mole fractions and ending with the one with the highest mole fractions. For each calibration cylinder, the entire first injection and the first 15 min of the subsequent injections are automatically rejected for equilibration time consideration. The instrument calibration takes 8 h and a linear fit is applied to compute the analyzer response. A target gas is automatically injected in the CRDS every 10 h for 30 min and again, the first 15 min are automatically rejected. The SDs at 1-sigma of the target gas analysis over one year were 0.02 µmol mol^{-1} for CO_2 and 0.14 nmol mol^{-1} for CH_4.

Ambient air is injected into the CRDS from the roof (through a 3/8 in decabon line, filtered using 3 filters of 7, 40 and 140 µm) using a pump located after the optical cavity. To avoid the risk of bias caused by interferences between water vapor and trace gases in the CRDS (Chen et al., 2010), the ambient air is dried prior to its injection into the CRDS by the drying system presented in Sect 3.1. A problem occurred in the cavity in August 2011, and the CRDS measurements were stopped until April 2012. The instrument has been returned to the manufacturer for repair.

3.3 Quality control of the GC system and comparisons with different analyzers

A target gas (TGT) is injected into the GC system once per hour for quality control. The target gas cylinder is a 40 L cylinder filled with dry ambient air at Gif-sur-Yvette. After stabilization for at least one month, the cylinder is analyzed at LSCE using the laboratory primary standards, and CO_2, CH_4, N_2O and SF_6 mole fraction values are assigned to the cylinder (see Table 4).

Figure 4 shows the time series of the target gas analysis from July 2010 to June 2013. The target gas cylinder was not changed over the three years. The different data gaps observed in CO_2 and CH_4 between March and October 2011 were caused by problems with the hydrogen generator (leaks in the electrolysis cell). The large data gaps in N_2O and SF_6 between April and August 2012 was due to a problem with the power supply of the Valco valve ♯1b. The reproducibility (computed here as the SD at 1-sigma of the target

analysis over one year of measurement) and the typical short-term repeatability (SD of the target analysis over 24 h) are presented in Table 5.

The vertical dark blue lines in Fig. 4 indicate when the working standards were changed and separate the two measurement periods: period A and period B (see Sect. 3.1.3). The average mole fractions of the TGT measurement during period A and period B are presented in Table 4 together with the respective assigned mole fractions. The measured CH_4, N_2O and SF_6 mole fractions agreed well with the assigned mole fractions during period A (considering the uncertainties). The respective difference between the CO_2 assigned and measured values in period A and period B were 0.15 and 0.19 $\mu mol\,mol^{-1}$ confirming the consistency between the two scales used in periods A and B. This agreement when using two different calibration scales shows that the problem is probably due to an error in the value attributed to this target gas. During period B, the average CH_4 mole fraction of the TGT gas was lower by approximately 10 $nmol\,mol^{-1}$ compared to period A. This decrease was due to a micro-leak in the WH line that was only detected in the CH_4 mole fractions because of the use of Ar/CH_4 as the carrier gas for the μECD. The use of this gas induces a larger CH_4 mole fraction in the laboratory than the ambient air level. Target data as well as ambient air measurements for this period should be re-calibrated by applying a one point calibration to the four trace gases. This micro-leak was fixed in September 2013, when the target cylinder was replaced by a new one (TG2).

In addition to internal quality control performed via the target gas analysis, comparisons of in situ ambient air analysis, flask analysis and cylinder analysis performed by different analyzers are relevant. These comparisons enable the validation of the scale consistency between different instruments and the detection of possible leaks or biases introduced by the inlet lines. The WMO-GAW recommends a scientific level of compatibility for such a comparison in the Northern Hemisphere (WMO-GAW, 2013). These levels are $\pm 0.1\ \mu mol\,mol^{-1}$ for CO_2, $\pm 2.0\ nmol\,mol^{-1}$ for CH_4, $\pm 0.1\ nmol\,mol^{-1}$ for N_2O and $\pm 0.02\ pmol\,mol^{-1}$ for SF_6.

The mean differences between the in situ GC system measurements and weekly flask sampling, in situ NDIR measurements and in situ CRDS measurements are summarized in Table 6. **These differences are calculated from the hourly mean measure-**

ments. A 2-sigma filter was applied to the differences to ~~prevent~~**flag the eventual** outliers. Comparisons between GC and NDIR were based on 9 months of overlapping measurements (July 2010 to April 2011) and revealed a mean CO_2 difference (GC minus NDIR) of $-0.14 \pm 1.78\,\mu mol\,mol^{-1}$. Comparisons between GC and CRDS were based on 20 months of overlapping measurements, from April 2011 to July 2013 with a break between August 2011 and April 2012. The average differences (GC minus CRDS) were $0.21 \pm 0.78\,\mu mol\,mol^{-1}$ for CO_2 and $-0.64 \pm 5.46\,nmol\,mol^{-1}$ for CH_4, over the total overlapping measurements. Because the CRDS instrument was stopped for several months and shipped to the manufacturer in 2011, we compared the results before and after its repair. In the first overlapping measurement period (April to August 2011), the differences were $-0.13 \pm 0.61\,\mu mol\,mol^{-1}$ and $-1.27 \pm 3.49\,nmol\,mol^{-1}$ for CO_2 and CH_4, respectively. In the second overlapping measurement period (April 2012 to July 2013) the CH_4 difference decreased to $-0.26 \pm 5.02\,nmol\,mol^{-1}$ whereas the CO_2 difference increased to $0.28 \pm 0.75\,\mu mol\,mol^{-1}$. Over the second comparison period, the observed CO_2 difference remained constant with time and did not depend on atmospheric mole fractions. The inlet lines, including the pumps and the dryer systems, were tested for three weeks: a common inlet line for ambient air measurements has been used for the GC and CRDS (the GC one, described in Sect. 3.1). During these three weeks of testing, the difference between GC and CRDS remained constant and equal to $0.28\,\mu mol\,mol^{-1}$, confirming that the inlet lines did not cause bias. Even after the change of the GC working standard in late April 2013, the CO_2 difference was still observed. **This observed difference is stable over time and is not concentration dependent. A second experiment was to analyze the second set of working standard on the CRDS. The results showed a difference between the assigned value (at LSCE) and the CRDS of $0.03\,\mu mol\,mol^{-1}$ on the WL and of $0.34\,\mu mol\,mol^{-1}$ on the WH.**

Comparisons between the GC system and the flask analysis or comparison cylinders provide information on the scale consistency between different laboratories. For the four analyzed long-lived GHGs, the comparisons between GC in situ measurements and flask analyses reached the desirable comparison levels (see Table 6 for more details). **The two**

GC measurements bracketing each sampled flask are linearly interpolated in order to match the time of the flask sampling. The Puy de Dôme station also participates in the "Cucumbers comparison programme" (http://cucumbers.uea.ac.uk/) in the frameworks of the European Union CarboEurope project (2000–2005), EU IMECC (2007–2011) and InGOS (2011–2015) infrastructure projects. Three cylinders are alternately analyzed on the GC at Puy de Dôme and at the Gif-sur-Yvette, Trainou (France), Kasprowy Wierch (Poland) and Hegyhatsal (Hungary) stations. Table 6 presents the mean differences between the average analysis of the 3 comparison cylinders at Puy de Dôme and Gif-sur-Yvette (LSCE) between 2011 and 2013. ~~With the exception of N_2O, for which the requested specification was not reached, the recommended comparison levels given by the WMO-GAW for CO_2, CH_4 and SF_6 were achieved.~~

The different comparison methods presented in this section showed that the GC system installed at Puy de Dôme station matches the WMO-GAW recommendations for CH_4 and SF_6 measurements. The CO_2 comparison shows different results depending on the method used. The recommendations are reached by considering the comparison with cylinders or flasks whereas it is not if we consider only the comparison between in-situ instruments. The WMO-GAW recommendations concerning the N_2O measurements are ambitious considering the repeatability obtained with our GC. The N_2O measurements do not reach the WMO-GAW recommendation but we can notice that the different comparison methods used show differences lower than our instrumental repeatability.

4 Results and discussions

4.1 Three years of ambient air measurements

Figure 5 shows the hourly time series of CO_2, CH_4, N_2O and SF_6 ambient air mole fractions together with the ^{222}Rn activities at Puy de Dôme from July 2010 to the end of June 2013. The different gaps observed in the atmospheric GHG time series were ex-

plained in Sect. 3.3. These time series are presented with the respective monthly background values (black lines). These monthly background values were calculated from the monthly average nighttime mole fractions (between 22:00 and 06:00 UTC), when the station is ~~usually~~ above the PBL (see Fig. 6). The hourly ^{222}Rn activities are presented in the last panel of Fig. 5 and varied between 0 and 9 Bq m^{-3} over the three years of measurements. From February 2012 to the end of April 2012, the computer for ^{222}Rn data acquisition had hardware and software problems, resulting in the observed gap.

Figure 6 presents the mean diurnal cycles per season of CO_2, CH_4, N_2O, SF_6, ^{222}Rn and for the PBL height (from ECMWF) from June 2010 to June 2013. **The GHG diurnal cycles were computed from the detrended hourly time series to the reference of January first, 2013. The mean yearly increase rate was subtracted from the time series, before computing the seasonal means diurnal cycles.** To represent the thickness of the PBL relative to the ground level, we used the altitude of Clermont-Ferrand (396 m a.s.l.) as the reference altitude to plot the PBL height because Clermont-Ferrand is located at the lowest altitude of the ECMWF extracted grid cell. The horizontal solid black line on the PBL height panel in Fig. 6 gives the altitude of the station above Clermont-Ferrand and enables a quick observation of whether the station is within or above the PBL. The mean diurnal cycles of the PBL height exhibited the same pattern for each season, with an increase in height from 06:00 to 12:00 UTC followed by a stable height until 16:00 UTC. After 16:00 UTC, the PBL height began to decrease, reaching a minimum after 20:00 UTC. On a mean annual scale, the GC sampled the trace gases within the PBL between 10:00 and 17:00 UTC with an enlarged time step in summer and a narrowed time step in winter. In winter, the Puy de Dôme station is often above the PBL during several consecutive days.

The mean diurnal cycles of the long-lived GHGs and ^{222}Rn observed in this study are the typical of mountain sites, as previously described by Schmidt et al. (1996) for the Schauinsland station (1205 m a.s.l.) or Necki et al. (2003) for the Kasprowy Wierch station (Poland, 1987 m a.s.l.). The PBL height is a key atmospheric factor, particularly for mountain sites where measurements alternate between the free troposphere and the PBL~~: atmospheric mole fractions of trace gases are generally lower in the free troposphere than in the PBL~~

~~because the sources are located at ground level~~. **The atmospheric mole fraction variabilities of trace gases are generally larger in the PBL because of the combination between its diurnal variability and the emissions from surface sources.** Due to its short radioactive lifetime, ^{222}Rn cannot accumulate in the free troposphere, in contrast to other long-lived trace gases. The mean diurnal cycles of ^{222}Rn (Fig. 6) exhibited larger variations in summer, when the PBL height is maximal and the inlet line of the station alternates between the PBL during daytime and above during nighttime. In winter, ^{222}Rn activities are lower than in summer because the station is usually in the free troposphere.

The mean diurnal cycles for CO_2 and CH_4 exhibited different shapes. As for the ^{222}Rn activities, the CH_4 mole fractions at the Puy de Dôme station were higher in the afternoon, when the PBL is well developed, compared with the night-time mole fractions. For the yearly average, CH_4 afternoon mole fractions were 3.3 nmol mol^{-1} higher than the night-time mole fractions. We observed an opposite diurnal cycle trend for CO_2: the biosphere is a sink for CO_2 during the daytime and counterbalances the atmospheric effects. This is clearly seen during summertime, when the photosynthetic activity is maximal: the amplitude of the CO_2 diurnal cycle was 7.2 µmol mol^{-1} with a minimum mole fraction around 16:00 UTC. The CO_2 mole fractions are maximal in winter when the biosphere acts as a CO_2 source, mainly driven by soil respiration.

The amplitudes of the N_2O and SF_6 diurnal cycles are very small and nearly undetectable**, except for the N_2O in summer which exhibits an amplitude of 0.25 nmol mol^{-1}**. The CH_4, N_2O and SF_6 mole fractions are largest in spring and lowest during summertime because their respective mole fractions are mainly driven by the PBL height and the associated vertical mixing.

4.2 The marine boundary layer reference

In this section, the background mole fractions of recorded trace gases at the station (see Sect. 4.1) are compared with the respective marine boundary layer references (MBLRs). Here, the MBLRs are the monthly zonal average trace gas mole fractions for a 45.5° N latitude computed from NOAA measurements: Dlugokencky et al. (2013a, b). They were

retrieved from the Global Monitoring Division of the NOAA Earth System Research Laboratory. Figure 7 shows the differences between the monthly mean background mole fractions at Puy de Dôme (night time values between 22:00 and 06:00 UTC) and the respective monthly MBLRs for CO_2, CH_4, N_2O and SF_6. These comparisons enable the direct quantification of the influence of sources and sinks on trace gases at the station relative to oceanic air masses. These differences are called continental offsets. The CO_2 continental offset has negative values in spring, indicating the influence of the continental biosphere, which acts as a sink. During summer, autumn and winter, the offsets are positive, revealing the importance of continental fossil fuel and biospheric sources in the Puy de Dôme catchment area. The continental offsets are usually positive for CH_4 but always positive for N_2O, indicating the strong influence of agricultural sources (see Sect. 2.1) in the Puy de Dôme footprint. Finally, the SF_6 offset varied between -0.10 and $+0.12\,\mathrm{pmol\,mol^{-1}}$, which represents the same order of magnitude as the GC measurement repeatability. In addition, Fig. 7 shows the monthly ^{222}Rn continental offset (for night-time selection data between 22:00 and 06:00 UTC) at Puy de Dôme station, relative to marine air. The marine air ^{222}Rn reference was computed from the mean activity of 15 years of measurements during maritime background condition at the European background site of Mace Head (see Bousquet et al., 1996) and is equal to $168\,\mathrm{mBq\,m^{-3}}$.

4.3 The radon tracer method

4.3.1 Method

Once emitted by soils, ^{222}Rn is an excellent tracer of continental air masses due to its physical and chemical properties. Thus the radon tracer method (RTM) has been used in numerous atmospheric studies to estimate trace gas surface emissions at the local to regional scales. Detailed descriptions of this method are given in the following studies: Schmidt et al. (2001); Hammer and Levin (2009); Yver et al. (2009); van der Laan et al. (2009a).

The RTM is based on Eq. (1), where J_x and J_{Rn} are the respective fluxes ~~densities~~ of a trace gas x and ^{222}Rn. The ΔC_x and ΔC_{Rn} terms are the temporal variations of the trace gas x mole fraction and of the ^{222}Rn activity over a period Δt. Finally, λ_{Rn} is the ^{222}Rn decay constant (Schmidt et al., 2001).

$$J_x = J_{\mathrm{Rn}} \frac{\Delta C_x}{\Delta C_{\mathrm{Rn}}} \left(1 - \frac{\lambda_{\mathrm{Rn}} C_{\mathrm{Rn}}}{\frac{\Delta C_{\mathrm{Rn}}}{\Delta t}} \right) \quad (1)$$

As shown in Fig. 6, the diurnal variations of trace gases at Puy de Dôme are very weak, which makes it difficult to correctly assess the ΔC_x and ΔC_{Rn} terms on a daily basis. In this study, we apply the RTM approach presented by Schmidt et al. (2003), in which the CO_2 fluxes ~~densities~~ at the Schauinsland station were calculated using the monthly CO_2 and ^{222}Rn continental offsets (relative to the MBLR). As presented in Sect 4.2, the continental offsets of trace gases reflect the source/sink influence at a continental site relative to a maritime background. In this study, the terms ΔC_x and ΔC_{Rn} (see Eq. 1) were calculated as the monthly offsets of trace gases and radon-222, respectively.

~~For a continental mountain site like Schauinsland,~~ Schmidt et al. (2003) ~~determined that the mean residence time for air masses over the European continent before reaching the station is 3 ± 1 days. This leads to a ^{222}Rn decay correction (term in brackets in Eq. 1 of 0.77. According to Fig. 1, most of the air masses arriving at the Puy de Dôme station and having a lifetime of three days are also from the continent.~~ **The term in brackets in Eq. 1 corresponds to the radioactive decay correction factor. For a continental mountain site like Schauinsland,** Schmidt et al. (2003) **determined that the mean residence time for air masses over the European continent before reaching the station is between 2 and 4 days, leading to a net effect of radioactive decay varying from 16 % to 29 %, respectively.** Based on the similarities between the Schauinsland and Puy de Dôme stations in terms of altitude, geographical position and continental air masses influence (Hammer et al., 2007; Lukács et al., 2007), the constant ^{222}Rn decay correction of 0.77 used for Schauinsland is also used for the Puy de Dôme station in this study.

The ^{222}Rn emission rate from continental surfaces strongly depends on the type and on the nature of the soils. A study of Karstens et al. (2015) provides a monthly ^{222}Rn emission map at $0.083^\circ \times 0.083^\circ$ over Europe. The assessment of this map takes into account the soil types and properties, the ^{238}U soil content and the soil moisture evolution over time. According to the mean nighttime footprint at the Puy de Dôme station (see Fig. 1b), we extracted the monthly ^{222}Rn average emission from this map for a 300 km $\times$ 300 km region centered on the Puy de Dôme station (U. Karstens and I. Levin, personal communication, 2014). Over the years 2010 to 2012, the ^{222}Rn fluxes range between 75 and 172 Bq m^{-2} h^{-1} with minimums in winter, when the soil is wet or frozen.

4.3.2 Uncertainties

The uncertainties of the radon tracer method presented above result from errors in the ^{222}Rn exhalation rate, errors in the ΔC_x and ΔC_{Rn} terms and error in the decay correction term (see Eq. 1). This section describes how these errors have been assessed to derive a mean relative uncertainty of the flux estimation of each trace gas.

A systematic assessment of the ^{222}Rn exhalation rates is quite difficult. The mean ratio of the spatial variability within the extracted area (300 km $\times$ 300 km region centered on the Puy de Dôme station) to the mean flux is 30 % (Karstens et al., 2015, and U. Karstens and I. Levin, personal communication, 2014). This number is used as a first approximation of the ^{222}Rn exhalation rates uncertainties. This estimate does not include systematic errors and therefore is likely an underestimate. Uncertainties in the ΔC_x term have been assessed from the MBLRs and from the background mole fractions uncertainties. The monthly MBLR uncertainties for CO_2 and CH_4 were provided by NOAA; mean uncertainties over the measurement period have been taken into account and are equal to 0.6 µmol mol^{-1} and 5.1 nmol mol^{-1}, respectively. We used a mean N_2O MBLR uncertainty of 0.3 nmol mol^{-1} which was estimated and provided by E. J. Dlugokencky (personal communication, 2014). The uncertainties on the background mole fractions at Puy de Dôme were derived directly from the respective GC repeatabilities (see Table 5). These last two error sources were combined to give the mean absolute continental offset (ΔC_x) over the entire measurement

period. Thus, the mean relative uncertainties in the continental offsets are estimated to be 31, 39 and 42 % for ΔC_{CO_2}, ΔC_{CH_4} and ΔC_{N_2O}, respectively. The ^{222}Rn instrument has an absolute error of $\pm$20 % for continental measurements (Biraud et al., 2000). Based on the same approach as for the ΔC_x term, a constant uncertainty of 28 % has been attributed to the ^{222}Rn continental offset term. Finally, Schmidt et al. (2003) reported an error of 7 % in the decay correction (term in brackets in Eq. 1).

These uncertainties were combined using the square root over the quadratic sum. The mean relative flux uncertainties derived for our RTM approach were 52, 57 and 59 % for CO_2, CH_4 and N_2O, respectively. The uncertainties estimated here using this continental RTM approach are larger than those found by Biraud et al. (2000), Schmidt et al. (2001), van der Laan et al. (2009a) or Lopez et al. (2012), which are all close to 35 % for the CO_2, CH_4 and N_2O flux estimates. The uncertainties presented here are mainly driven by the continental offset uncertainties.

The uncertainties in the SF_6 emissions are up to 300 %. Therefore we do not present any SF_6 emissions in this study.

4.3.3 Estimation of GHG surface fluxes in the Puy de Dôme catchment area

Continental CO_2, CH_4 and N_2O surface fluxes were calculated using the radon tracer method at the Puy de Dôme station. As shown by Gloor et al. (2001), the knowledge of the station footprint is an important parameter in interpreting the large time variability of a trace gas mole fraction observed at a measurement station. Figure 1b shows the integrated nighttime footprint (22:00 to 06:00 UTC) of the Puy de Dôme station between 2010 and 2013 (see Sect. 2.2 for more details). The station is mainly influenced by regional air masses, which are well distributed all around the station during nighttime, when the measurements are usually performed in the free troposphere.

The calculated monthly fluxes are presented in Fig. 8 together with the hourly ^{222}Rn exhalation rate (U. Karstens and I. Levin, personal communication, 2014) at Puy de Dôme. The units used to express the trace gas fluxes are: $\mathrm{t\,km^{-2}\,month^{-1}}$ for CO_2 and CH_4 and $\mathrm{kg\,km^{-2}\,month^{-1}}$ for N_2O. Because no ^{222}Rn activities were recorded between January

and the end of April 2012, no fluxes could be derived from the RTM. The vertical grey lines on each curve are the ~~relative~~ **absolute** uncertainties calculated in Sect. 4.3.2.

The CO_2 fluxes integrate the signals from all CO_2 sources and sinks in the night-time footprint of the station. These are the contributions of the biosphere (emissions and uptakes) and of the anthropogenic emissions (fossil fuel and biofuel). The derived CO_2 fluxes present negative values in spring, emphasizing the net uptake by the plant assimilation with a monthly average value between April and June of $-382 \pm 198\,\mathrm{t(CO_2)\,km^{-2}\,month^{-1}}$ in the station catchment area. Schmidt et al. (2003) calculated CO_2 fluxes at the Schauinsland station from 1980 to 2000 and observed a long-term monthly mean CO_2 uptake between May and June of $147\,\mathrm{t(CO_2)\,km^{-2}}$, with a maximum uptake of $550\,\mathrm{t(CO_2)\,km^{-2}}$ in spring 1989. These values are the same order of magnitude as the estimations of this study. In summer, fall and winter, the fluxes are positive, indicating that the CO_2 signal is dominated by the biospheric (predominantly soil respiration) and fossil fuel emissions. The monthly average CO_2 flux over the total measurement period in the Puy de Dôme station footprint is $96 \pm 50\,\mathrm{t(CO_2)\,km^{-2}\,month^{-1}}$. The CITEPA (French emission inventory) provides only anthropogenic emissions for the Auvergne region, which is $21\,\mathrm{t(CO_2)\,km^{-2}\,month^{-1}}$. Our approach can not separate biospheric sources and fossil fuel sources; therefore, a direct comparison between the atmospheric approach and the emission inventory is not possible.

The CH_4 fluxes exhibit large variabilities, with monthly values between -0.91 ± 0.52 and $1.45 \pm 0.82\,\mathrm{t(CH_4)\,km^{-2}\,month^{-1}}$. Negative values occurred in April, September and November 2011 **Negative values occurred in April, September and November 2011 due to biases in the calculated background induced by the many data gaps during the considered months. Therefore, these negative fluxes are not taken into account in the average flux calculation.**. The averageCH_4 emission was $6.2 \pm 3.5\,\mathrm{t(CH_4)\,km^{-2}\,yr^{-1}}$ over the total measurement period. The N_2O estimate emissions varies between 74 ± 44 and$316 \pm 187\,\mathrm{kg(N_2O)\,km^{-2}\,month^{-1}}$, with a mean annual emission of $1546 \pm 912\,\mathrm{kg(N_2O)\,km^{-2}\,yr^{-1}}$.

Several studies have used the radon tracer method to estimate CH_4 and/or N_2O emissions over Western Europe: Biraud et al. (2000); Schmidt et al. (2001); Lopez et al. (2012).

The results of these estimations are summarized in Table 7 together with the CH_4 and N_2O emissions estimated by this study and the estimate provided by the CITEPA for the Auvergne region. The estimates of CH_4 emissions in the cited literature agree well over western Europe, with the exception of the estimation of van der Laan et al. (2009a), who calculated much higher CH_4 emissions for the Netherlands. **Following Figure 1, the grid cells contributing the most to the signal measured at the station at night cover an area of approximately $300\,\mathbf{km} \times 300\,\mathbf{km}$. The Auvergne region covers an area of approximately $150\,\mathbf{km} \times 250\,\mathbf{km}$ also centered in the station but the neighboring regions are also rural area presenting roughly the same land cover and similar GHG fluxes which allows a direct *comparison between the fluxes estimated by our atmospheric approach and those estimated by the CITEPA for the Auvergne region.**

The CITEPA estimates a yearly CH_4 emission of $6.0\,t(CH_4)\,km^{-2}\,yr^{-1}$ for the Auvergne region, indicating a good agreement between the inventory and the atmospheric approach. However, our study overestimates the N_2O emissions by a factor of five compared with the CITEPA estimations. The N_2O flux is mainly driven by agricultural sources in the Auvergne region (CITEPA, 2010), and such fluxes strongly depend on the soil characteristics, soil temperature, and amount and type of fertilizer used. Thus, soil N_2O emissions are extremely heterogeneous, which explains the distribution of results obtained in the different cited studies in Table 7. The high N_2O emissions observed in this study may be attributable to the influence of a local agricultural source. These differences are also linked to significant uncertainties, which are strongly driven by the small continental offsets between 0.6 and $1.5\,nmol\,mol^{-1}$. Despite this difference, the presented atmospheric approach provides an independent estimation of GHG emission over the station footprint as well as new information on flux seasonality ~~with lower fluxes as expected~~.

5 Conclusions

Semi-continuous measurements of four long-lived GHGs at Puy de Dôme started in 2010 with the installation of a GC system. This GC was designed to automatically measure CO_2,

CH_4, N_2O and SF_6 atmospheric mole fractions. ~~Many comparisons between the in situ GC system and the GC system located at LSCE (Gif-sur-Yvette) via flask or cylinder analysis showed comparison levels in agreement with those recommended by the WMO-GAW. The comparisons between the GC and CRDS in situ measurements indicated a high degree of compatibility for CH_4 whereas a constant offset of 0.21 µmol mol^{-1} was observed for CO_2 ambient air comparison.~~ **We described in details three methods which have been used for comparison purposes. They are based on direct comparison between two in-situ analyzers, flask measurements and cylinder measurements. For CH_4 and SF_6, all comparisons show that GC measurements at Puy de Dôme are in agreement with the WMO-GAW compatibility goals. For N_2O, our measurements do not match the ambitious WMO-GAW compatibility goal. For CO_2, the comparison based on ambient air flasks and reference cylinders analysis between the GCs operated at Puy de Dôme and at LSCE reaches the desirable comparison level showing there is no bias in the scale transfer between the two sites. Nevertheless, it does not for the in-situ comparison with other analyzers (NDIR and CRDS). The comparisons between the GC and the CRDS in-situ measurements indicated a constant offset of 0.21 µmol mol^{-1} CO_2 over 20 months of overlapping measurements.** Several tests have been performed and explained in the study, but the reason for the observed constant bias is not yet clear. We continue to work on this issue and are therefore aware of the order of magnitude of bias that is possible.

At stations that typically run only one analyzer, a bias of 0.25 µmol mol^{-1} might not be detected when the target gas and the comparison cylinders yield good results. **For consistency reasons, we thus recommend to use different methods based on flask or cylinder comparisons but also based on in-situ comparisons to check if the considered measurements match with the WMO-GAW recommendations.**

The diurnal cycles of CO_2 and CH_4 at Puy de Dôme are mainly driven by the PLB height, and they present the typical shape of a mountain station, such as the Schauinsland or Kasprowy Wierch stations, while the N_2O and SF_6 mean diurnal cycles present flat behaviors that are difficult to interpret.

Radon-222 was used in this study as an air mass tracer to estimate the monthly continental fluxes ~~densities~~ of CO_2, CH_4 and N_2O relative to the maritime background layer references. We derived a yearly net emission of $1150\,t(CO_2)\,km^{-2}$, $6.2\,t(CH_4)\,km^{-2}$ and $1.5\,t(N_2O)\,km^{-2}$. The derived CO_2 and CH_4 fluxes compare well with other European studies or with the national inventory (CITEPA). However, it remains difficult to compare the N_2O fluxes with other studies due to large errors. ~~In the future, new analysis techniques based on CRDS, FTIR or OA-ICOS will help achieve better precision and fewer data gaps at remote stations with only weekly maintenance visits, which will further improve uncertainties in flux estimates.~~ **Compare to the GC system presented in this study, the new analysis technique based on CRDS, FTIR or OA-ICOS achieve better precision and require less maintenance. In consequence, the use of these new technologies enables the development of dense measurement network, such as ICOS, which will further improve uncertainties in the flux estimates.**

Acknowledgements. The authors thank the LaMP team for weekly maintenance of the station and weekly flask sampling. We also acknowledge the support provided by the RAMCES group at LSCE for regular maintenance of the analyzer and for data management. We thank the ECWMF and I. Pison for providing and extracting the meteorological conditions at the Puy de Dôme pixel. We also want to thank I. Levin and U. Karstens for providing and sharing the European ^{222}Rn map emissions. We used the marine boundary layer reference kindly provided by E. Dlugokencky and K. Masarie from NOAA. The authors acknowledge the Regional Council of Auvergne for the financial support. This work was partly funded by the InGOS EU project (284274).

References

Biraud, S., Ciais, P., Ramonet, M., Simmonds, P., Kazan, V., Monfray, P., O'Doherty, S., Spain, T. G., and Jennings, S. G.: European greenhouse gas emissions estimated from continuous atmospheric measurements and radon 222 at Mace Head, Ireland, J. Geophys. Res.-Atmos., 105, 1351–1366, doi:10.1029/1999JD900821, 2000.

Boulon, J., Sellegri, K., Hervo, M., Picard, D., Pichon, J.-M., Fréville, P., and Laj, P.: Investigation of nucleation events vertical extent: a long term study at two different altitude sites, Atmos. Chem. Phys., 11, 5625–5639, doi:10.5194/acp-11-5625-2011, 2011.

Bousquet, P., Gaudry, A., Ciais, P., Kazan, V., Monfray, P., Simmonds, P. G., Jennings, S. G., and O'Connor, T. C.: Atmospheric CO_2 concentration variations recorded at Mace Head, Ireland, from 1992 to 1994, Phys. Chem. Earth, 21, 477–481, 1996.

Chen, H., Winderlich, J., Gerbig, C., Hoefer, A., Rella, C. W., Crosson, E. R., Van Pelt, A. D., Steinbach, J., Kolle, O., Beck, V., Daube, B. C., Gottlieb, E. W., Chow, V. Y., Santoni, G. W., and Wofsy, S. C.: High-accuracy continuous airborne measurements of greenhouse gases (CO_2 and CH_4) using the cavity ring-down spectroscopy (CRDS) technique, Atmos. Meas. Tech., 3, 375–386, doi:10.5194/amt-3-375-2010, 2010.

CITEPA: Inventaire régional d'émission de polluants atmosphériques et de gaz à effet de serre dans le cadre du schéma régional Climat-Air-Energie, Auvergne, Tech. rep., CITEPA, Paris, France, 2010.

Collins, M., Knutti, R., Arblaster, J., Dufresne, J.-L., Fichefet, T., Friedlingstein, P., Ga, X., Gutowski, W. J., Johns, T., Krinner, G., Shongwe, M., Tebaldi, C., Weaver, A. J., and Wehner, M.: Long-term climate change: projections, commitments and irreversibility, in: Climate Change 2013: The Physical Science Basis. Contribution of Working Group I to the Fifth Assessment Report of the Intergovernmental Panel on Climate Change, edited by: Stocker, T. F., Qin, D., Plattner, G.-K., Tignor, M., Allen, S. K., Boschung, J., Nauels, A., Xia, Y., Bex, V., and Midgley, P. M., Cambridge University Press, United Kingdom and New York, USA, chapter 12, 2013.

Dlugokencky, E. J., Myers, R. C., Lang, P. M., Masarie, K. A., Crotwell, A. M., Thoning, K. W., Hall, B. D., Elkins, J. W., and Steele, L. P.: Conversion of NOAA atmospheric dry air CH_4 mole fractions to a gravimetrically prepared standard scale, J. Geophys. Res.-Atmos., 110, D18306, doi:10.1029/2005JD006035, 2005.

Dlugokencky, E. J., Lang, P. M., Crotwell, A. M., Masarie, K. A., and Crotwell, M. J.: Atmospheric Methane Dry Air Mole Fractions from the NOAA ESRL Carbon Cycle Cooperative Global Air Sampling Network, 1983–2012, Version: 2013-08-28, available at: ftp://aftp.cmdl.noaa.gov/data/trace_gases/ch4/flask/surface (last access: 18 March 2015), 2013a.

Dlugokencky, E. J., Masarie, K. A., Lang, P. M., and Tans, P. P.: NOAA Greenhouse Gas Reference from Atmospheric Carbon Dioxide Dry Air Mole Fractions from the NOAA ESRL Carbon Cycle Cooperative Global Air Sampling Network, available at: ftp://aftp.cmdl.noaa.gov/data/trace_gases/co2/flask/surface (last access: 18 March 2015), 2013b.

ECMWF: IFS documentation CY38r1, part IV: physical processes, Tech. rep., ECMWF, available at: https://software.ecmwf.int/wiki/display/IFS/ (last access: 18 March 2015), 2012.

Forster, P., Ramaswamy, V., Artaxo, P., Berntsen, T., Betts, R., Fahey, D. W., Haywood, J., Lean, J., Lowe, D. C., Myhre, G., Nganga, J., Prinn, R., Schultz, M., and Dorland, R. V.: Changes in atmospheric constituents and in radiative forcing, in: Climate change 2007: The physical science basis. Contribution of Working Group I to the Fourth Assessment Report of the Intergovernmental Panel on Climate Change , edited by Solomon, S., Qin, D., Manning, M., Chen, Z., Marquis, M., Averyt, K. B., Tignor, M., and Miller, H. L., pp. 129–234, Cambridge University Press, 2007.

Gloor, M., Bakwin, P., Hurst, D., Lock, L., Draxler, R., and Tans, P.: What is the concentration footprint of a tall tower?, J. Geophys. Res.-Atmos., 106, 17831–17840, doi:10.1029/2001JD900021, 2001.

Hall, B. D., Dutton, G. S., and Elkins, J. W.: The NOAA nitrous oxide standard scale for atmospheric observations, J. Geophys. Res.-Atmos., 112, D09305, doi:10.1029/2006JD007954, 2007.

Hammer, S., Wagenbach, D., Preunkert, S., Pio, C., Schlosser, C., and Meinhardt, F.: Lead-210 observations within CARBOSOL: A diagnostic tool for assessing the spatiotemporal variability of related chemical aerosol species?, Journal of Geophysical Research: Atmospheres, 112, n/a–n/a, doi:10.1029/2006JD008065, http://dx.doi.org/10.1029/2006JD008065, d23S03, 2007.

Hammer, S. and Levin, I.: Seasonal variation of the molecular hydrogen uptake by soils inferred from continuous atmospheric observations in Heidelberg, southwest Germany, Tellus B, 61, 556–565, doi:10.1111/j.1600-0889.2009.00417.x, 2009.

Hammer, S., Griffith, D. W. T., Konrad, G., Vardag, S., Caldow, C., and Levin, I.: Assessment of a multi-species in situ FTIR for precise atmospheric greenhouse gas observations, Atmos. Meas. Tech., 6, 1153–1170, doi:10.5194/amt-6-1153-2013, 2013a.

Hammer, S., Konrad, G., Vermeulen, A. T., Laurent, O., Delmotte, M., Jordan, A., Hazan, L., Conil, S., and Levin, I.: Feasibility study of using a "travelling" CO_2 and CH_4 instrument to validate continuous in situ measurement stations, Atmos. Meas. Tech., 6, 1201–1216, doi:10.5194/amt-6-1201-2013, 2013b.

Hartmann, D. L., Klein-Tank, A. M. G., Rusticucci, M., Alexander, L. V., Brönnimann, S., Charabi, Y., Dentener, F. J., Dlugokencky, E. J., Easterling, D. R., Kaplan, A., Soden, B. J., Thorne, P. W., Wild, M., and Zhai, P. M.: Observations: atmosphere and surface, in: Climate Change 2013: The Physical Science Basis. Contribution of Working Group I to the Fifth Assessment Report of the Intergovernmental Panel on Climate Change, edited by: Stocker, T. F., Qin, D., Plattner, G.-K., Tignor, M., Allen, S. K., Boschung, J., Nauels, A., Xia, Y., Bex, V., and Midgley, P. M., Cambridge University Press, United Kingdom and New York, USA, 159–254, 2013.

Karstens, U., Schwingshackl, C., Schmithüsen, D., and Levin, I.: A process-based ^{222}Rn flux map for Europe and its comparison to long-term observations, Atmospheric Chemistry and Physics Discussions, 15, 17 397–17 448, doi:10.5194/acpd-15-17397-2015, http://www.atmos-chem-phys-discuss.net/15/17397/2015/, 2015.

Keeling, C. D.: The concentration and isotopic abundances of carbon dioxide in the atmosphere, Tellus, 12, 200–203, doi:10.1111/j.2153-3490.1960.tb01300.x, 1960.

Keeling, C. D., Bacastow, R. B., Bainbridge, A. E., Ekdahl, C. A., Guenther, P. R., Waterman, L. S., and Chin, J. F. S.: Atmospheric carbon dioxide variations at Mauna Loa Observatory, Hawaii, Tellus, 28, 538–551, doi:10.1111/j.2153-3490.1976.tb00701.x, 1976.

Levin, I. and Karsten, U.: Inferring high-resolution fossil fuel CO_2 records at continental sites from combined $^{14}CO_2$ and CO observations, Tellus B, 59, 245–250, doi:10.1111/j.1600-0889.2006.00244.x, 2007.

Levin, I., Naegler, T., Heinz, R., Osusko, D., Cuevas, E., Engel, A., Ilmberger, J., Langenfelds, R. L., Neininger, B., Rohden, C. v., Steele, L. P., Weller, R., Worthy, D. E., and Zimov, S. A.: The global SF_6 source inferred from long-term high precision atmospheric measurements and its comparison with emission inventories, Atmos. Chem. Phys., 10, 2655–2662, doi:10.5194/acp-10-2655-2010, 2010.

Lin, J. C., Gerbig, C., Wofsy, S. C., Andrews, A. E., Daube, B. C., Davis, K. J., and Grainger, C. A.: A near-field tool for simulating the upstream influence of atmospheric observations: the Stochastic Time-Inverted Lagrangian Transport (STILT) model, J. Geophys. Res.-Atmos., 108, 4493, doi:10.1029/2002JD003161, 2003.

Lopez, M.: Estimation des émissions de gaz à effet de serre à différentes échelles en France à l'aide d'observations de haute précision., Ph.D. thesis, available at: https://tel.archives-ouvertes.fr/tel-00777476 (last access: 18 March 2015), 2012.

Lopez, M., Schmidt, M., Yver, C., Messager, C., Worthy, D., Kazan, V., Ramonet, M., Bousquet, P., and Ciais, P.: Seasonal variation of N_2O emissions in France inferred from atmospheric N_2O and ^{222}Rn measurements, J. Geophys. Res.-Atmos., 117, D14103, doi:10.1029/2012JD017703, 2012.

Lopez, M., Schmidt, M., Delmotte, M., Colomb, A., Gros, V., Janssen, C., Lehman, S. J., Mondelain, D., Perrussel, O., Ramonet, M., Xueref-Remy, I., and Bousquet, P.: CO, NO_x and $^{13}CO_2$ as tracers for fossil fuel CO_2: results from a pilot study in Paris during winter 2010, Atmos. Chem. Phys., 13, 7343–7358, doi:10.5194/acp-13-7343-2013, 2013.

Lukács, H., Gelencsér, A., Hammer, S., Puxbaum, H., Pio, C., Legrand, M., Kasper-Giebl, A., Handler, M., Limbeck, A., Simpson, D., and Preunkert, S.: Seasonal trends and possible sources of brown carbon based on 2-year aerosol measurements at six sites in Europe, Journal of Geophysical Research: Atmospheres, 112, n/a–n/a, doi:10.1029/2006JD008151, http://dx.doi.org/10.1029/2006JD008151, d23S18, 2007.

Maiss, M., Steele, L., Francey, R. J., Fraser, P. J., Langenfelds, R. L., Trivett, N. B., and Levin, I.: Sulfur hexafluoride – a powerful new atmospheric tracer, Atmos. Environ., 30, 1621–1629, doi:10.1016/1352-2310(95)00425-4, 1996.

Myhre, G., Shindell, D., Bréon, F.-M., Collins, W., Fuglestvedt, J., Huang, J., Koch, D., Lamarque, J.-F., Lee, D., Mendoza, B., Nakajima, T., Robock, A., Stephens, G., Takemura, T., and Zhang, H.: Anthropogenic and natural radiative forcing, in: Climate Change 2013: The Physical Science Basis. Contribution of Working Group I to the Fifth Assessment Report of the Intergovernmental Panel on Climate Change, edited by: Stocker, T. F., Qin, D., Plattner, G.-K., Tignor, M., Allen, S. K., Boschung, J., Nauels, A., Xia, Y., Bex, V., and Midgley, P. M., Cambridge University Press, United Kingdom and New York, USA, chapter 8, 2013.

Miller, J. B., Lehman, S. J., Montzka, S. A., Sweeney, C., Miller, B. R., Karion, A., Wolak, C., Dlugokencky, E. J., Southon, J., Turnbull, J. C., and Tans, P. P.: Linking emissions of fossil fuel CO_2 and other anthropogenic trace gases using atmospheric $^{14}CO_2$, J. Geophys. Res.-Atmos., 117, D08302, doi:10.1029/2011JD017048, 2012.

Necki, J., Schmidt, M., Rozanski, K., Zimnoch, M., Korus, A., Lasa, J., Graul, R., and Levin, I.: Six-year record of atmospheric carbon dioxide and methane at a high-altitude mountain site in Poland, Tellus B, 55, 94–104, doi:10.1034/j.1600-0889.2003.01446.x, 2003.

Polian, G., Lambert, G., Ardouin, B., and Jegou, A.: Long-range transport of continental radon in subantarctic and antarctic areas, Tellus B, 38, 178–189, doi:10.1111/j.1600-0889.1986.tb00185.x, 1986.

Popa, M. E., Gloor, M., Manning, A. C., Jordan, A., Schultz, U., Haensel, F., Seifert, T., and Heimann, M.: Measurements of greenhouse gases and related tracers at Bialystok tall tower station in Poland, Atmos. Meas. Tech., 3, 407–427, doi:10.5194/amt-3-407-2010, 2010.

Prinn, R., Cunnold, D., Rasmussen, R., Simmonds, P., Alyea, F., Crawford, A., Fraser, P., and Rosen, R.: Atmospheric emissions and trends of nitrous oxide deduced from 10 years of ALE–GAGE data, J. Geophys. Res.-Atmos., 95, 18369–18385, doi:10.1029/JD095iD11p18369, 1990.

Rasmussen, R. A. and Khalil, M. A. K.: Atmospheric methane (CH_4): trends and seasonal cycles, J. Geophys. Res.-Oceans, 86, 9826–9832, doi:10.1029/JC086iC10p09826, 1981.

Schmidt, M.: Messung und Bilanzierung anthropogener Treibhausgase in Deutschland, PhD thesis, University of Heidelberg, Heidelberg, 1999.

Schmidt, M., Graul, R., Sartorius, H., and Levin, I.: Carbon dioxide and methane in continental Europe: a climatology, and ^{222}Radon-based emission estimates, Tellus B, 48, 457–473, doi:10.1034/j.1600-0889.1994.t01-2-00002.x-i1, 1996.

Schmidt, M., Glatzel-Mattheier, H., Sartorius, H., Worthy, D. E., and Levin, I.: Western European N_2O emissions: a top-down approach based on atmospheric observations, J. Geophys. Res.-Atmos., 106, 5507–5516, doi:10.1029/2000JD900701, 2001.

Schmidt, M., Graul, R., Sartorius, H., and Levin, I.: The Schauinsland CO_2 record: 30 years of continental observations and their implications for the variability of the European CO_2 budget, J. Geophys. Res.-Atmos., 108, 4619, doi:10.1029/2002JD003085, 2003.

Schmidt, M., Lopez, M., Yver Kwok, C., Messager, C., Ramonet, M., Wastine, B., Vuillemin, C., Truong, F., Gal, B., Parmentier, E., Cloué, O., and Ciais, P.: High-precision quasi-continuous atmospheric greenhouse gas measurements at Trainou tower (Orléans forest, France), Atmos. Meas. Tech., 7, 2283–2296, doi:10.5194/amt-7-2283-2014, 2014.

Seidel, D. J., Zhang, Y., Beljaars, A., Golaz, J.-C., Jacobson, A. R., and Medeiros, B.: Climatology of the planetary boundary layer over the continental United States and Europe, J. Geophys. Res.-Atmos., 117, D17106, doi:10.1029/2012JD018143, 2012.

Thompson, R. L., Manning, A. C., Gloor, E., Schultz, U., Seifert, T., Hänsel, F., Jordan, A., and Heimann, M.: In-situ measurements of oxygen, carbon monoxide and greenhouse gases from Ochsenkopf tall tower in Germany, Atmos. Meas. Tech., 2, 573–591, doi:10.5194/amt-2-573-2009, 2009.

Thoning, K. W., Tans, P. P., and Komhyr, W. D.: Atmospheric carbon dioxide at Mauna Loa Observatory: 2. Analysis of the NOAA GMCC data, 1974–1985, J. Geophys. Res.-Atmos., 94, 8549–8565, doi:10.1029/JD094iD06p08549, 1989.

Turnbull, J. C., Tans, P. P., Lehman, S. J., Baker, D., Conway, T. J., Chung, Y. S., Gregg, J., Miller, J. B., Southon, J. R., and Zhou, L.-X.: Atmospheric observations of carbon monoxide and fossil fuel CO_2 emissions from East Asia, J. Geophys. Res.-Atmos., 116, D24306, doi:10.1029/2011JD016691, 2011.

Turner, D. B.: A diffusion model for an urban area, J. Appl. Meteorol., 3, 83–91, 1964.

van der Laan, S., Neubert, R. E. M., and Meijer, H. A. J.: Methane and nitrous oxide emissions in The Netherlands: ambient measurements support the national inventories, Atmos. Chem. Phys., 9, 9369–9379, doi:10.5194/acp-9-9369-2009, 2009a.

van der Laan, S., Neubert, R. E. M., and Meijer, H. A. J.: A single gas chromatograph for accurate atmospheric mixing ratio measurements of CO_2, CH_4, N_2O, SF_6 and CO, Atmos. Meas. Tech., 2, 549–559, doi:10.5194/amt-2-549-2009, 2009b.

Venzac, H., Sellegri, K., Villani, P., Picard, D., and Laj, P.: Seasonal variation of aerosol size distributions in the free troposphere and residual layer at the puy de Dôme station, France, Atmos. Chem. Phys., 9, 1465–1478, doi:10.5194/acp-9-1465-2009, 2009.

Weiss, R. F.: The temporal and spatial distribution of tropospheric nitrous oxide, J. Geophys. Res.-Oceans, 86, 7185–7195, doi:10.1029/JC086iC08p07185, 1981.

WMO-GAW (Ed.): Global atmosphere watch measurements guide – global atmosphere watch report series No. 143, WMO-TD 1073, Global Atmosphere Watch, Geneva, 2001.

WMO-GAW (Ed.): 17th WMO/IAEA Meeting of Experts on Carbon Dioxide, Other Greenhouse Gases, and Related Tracer Measurement Techniques, vol. 213, Global Atmosphere Watch, Beijing, China, 10–14 June 2013.

Xia, Y., Sartorius, H., Schlosser, C., Stöhlker, U., Conen, F., and Zahorowski, W.: Comparison of one- and two-filter detectors for atmospheric ^{222}Rn measurements under various meteorological conditions, Atmos. Meas. Tech., 3, 723–731, doi:10.5194/amt-3-723-2010, 2010.

Yver, C., Schmidt, M., Bousquet, P., Zahorowski, W., and Ramonet, M.: Estimation of the molecular hydrogen soil uptake and traffic emissions at a suburban site near Paris through hydrogen, carbon monoxide, and radon-222 semicontinuous measurements, J. Geophys. Res., 114, D18304, doi:10.1029/2009JD012122, 2009.

Yver Kwok, C., Laurent, O., Guemri, A., Philippon, C., Wastine, B., Rella, C. W., Vuillemin, C., Truong, F., Delmotte, M., Kazan, V., Darding, M., Lebègue, B., Kaiser, C., and Ramonet, M.: Comprehensive laboratory and field testing of cavity ring-down spectroscopy analyzers measuring H_2O, CO_2, CH_4 and CO, Atmospheric Measurement Techniques Discussions, 8, 4219–4272, doi:10.5194/amtd-8-4219-2015, http://www.atmos-meas-tech-discuss.net/8/4219/2015/, 2015.

Zhao, C. L. and Tans, P. P.: Estimating uncertainty of the WMO mole fraction scale for carbon dioxide in air, J. Geophys. Res.-Atmos., 111, D08S09, doi:10.1029/2005JD006003, 2006.

Table 1. Measurement method used for the GC system at the Puy de Dôme station. **The "On" position on the valves presented here corresponds to the dashed lines in Fig. 2 and the "Off" position correspond to the solid lines.**

Time (min)	Parameter	Value	Comments
0.00	Aux 3	45.0 psi	Carrier gas pressure for N_2
0.00	Aux 4	20.0 psi	Carrier gas pressure for Ar/CH_4
0.00	Aux 5	2.5 psi	Sample pressure
0.00	Valve ♯1	On	Flush of the sample loops
0.00	Valve ♯3	On	Backflush of the pre-column (N_2O/SF_6)
0.75	Aux 5	0.0 psi	Sample pressure
0.75	Valve ♯3	Off	Stop of pre-column backflushing
1.25	Valve ♯1	Off	Sample injection
3.10	Valve ♯4	On	Injection of CO_2 in the catalyst
3.60	Aux 3	0.0 psi	Carrier gas pressure for N_2
3.70	Valve ♯3	On	Backflush of the pre-column
5.30	Valve ♯4	Off	Switch of the catalyst valve
5.40	Aux 3	45.0 psi	Carrier gas pressure for Ar/CH_4

Table 2. GC system equipment and temperature and flow rate settings.

Detector	FID (CO_2/CH_4)	μECD (N_2O/SF_6)
Carrier gas	N_2 cylinder (purity > 99,9999 %) + purifier	Ar/CH_4 cylinder (ECD quality) + purifier
Flow rate	100 mL min^{-1}	45/65 mL min^{-1}
Loop sample volume	15 mL	10 mL
Oven temperature	80 °C	80 °C
Pre-column		Hayesep-Q $4' \times 3/16''$SS, 80/100
Analytical column	Hayesep-Q $12' \times 3/16''$SS, 80/100	Hayesep-Q $6' \times 3/16''$SS, 80/100
Detector temperature	300 °C	395 °C
Catalyst temperature	390 °C	
Gas supply	H_2 generator: 60 mL min^{-1} Air zero generator: 400 mL min^{-1}	

Table 3. Trace gas mole fractions of GC working standards used during period A (July 2010 to April 2013) and period B (May and June 2013).

Species	Period A – 33 months		Period B – 2 months	
	WH	WL	WH	WL
CO_2 ($\mu mol\,mol^{-1}$)	425.10	372.45	449.60	363.31
CH_4 ($nmol\,mol^{-1}$)	2179.90	1732.99	2083.38	1663.52
N_2O ($nmol\,mol^{-1}$)	340.90	322.93	348.03	326.51
SF_6 ($pmol\,mol^{-1}$)	10.05	5.38	9.86	5.86

Table 4. Assigned target gas values with the respective mole fractions measured using the GC system at the Puy de Dôme station over period A and period B. The assigned values were measured by the GC system at the LSCE central lab against WMO calibration gases.

Species	Assigned values	Period A	Period B
CO_2 ($\mu mol\,mol^{-1}$)	402.57 ± 0.07	402.42 ± 0.15	402.38 ± 0.46
CH_4 ($nmol\,mol^{-1}$)	1973.87 ± 0.73	1973.81 ± 2.12	1963.72 ± 6.64
N_2O ($nmol\,mol^{-1}$)	325.71 ± 0.23	325.90 ± 0.35	325.76 ± 0.47
SF_6 ($pmol\,mol^{-1}$)	7.23 ± 0.04	7.23 ± 0.06	7.20 ± 0.07

Table 5. Reproducibility and typical short-term (24 h) repeatability of the GC system at Puy de Dôme, both at 1-sigma.

Species	Reproducibility	Short-term repeat
CO_2 ($\mu mol\ mol^{-1}$)	0.14	0.1
CH_4 ($nmol\ mol^{-1}$)	2.12	1.2
N_2O ($nmol\ mol^{-1}$)	0.34	0.3
SF_6 ($pmol\ mol^{-1}$)	0.06	0.06

Table 6. Results of the comparisons between in situ measurements obtained using the GC system, NDIR, CRDS and flask measurements. The mean differences in the cylinder analysis at the Puy de Dôme and Gif-sur-Yvette stations are presented in the last column. Flasks and cylinders were analyzed at the LSCE central lab at Gif-sur-Yvette.

Date Comparisons	Jul 2010–Jul 2013 GC in situ – flasks Average	 Nb of flasks	Jul 2010–Apr 2011 In situ: GC-NDIR	Apr 2011–Jul 2013 In situ: GC-CRDS	Jul 2010–Jul 2013 Cylinders: PUY-GIF
CO_2 (μmol mol^{-1})	0.11 ± 1.19	55	-0.14 ± 1.78	0.21 ± 0.78	-0.02 ± 0.11
CH_4 (nmol mol^{-1})	0.04 ± 4.30	57	NA	-0.64 ± 5.46	0.64 ± 0.26
N_2O (nmol mol^{-1})	0.12 ± 0.55	47	NA	NA	0.21 ± 0.47
SF_6 (pmol mol^{-1})	-0.01 ± 0.07	53	NA	NA	0.03 ± 0.03

Table 7. Summary of CH_4 and N_2O fluxes estimations and their respective uncertainties over Western Europe using the RTM (this study, Biraud et al., 2000; Schmidt et al., 2001; van der Laan et al., 2009a; Lopez et al., 2012, and regional emission inventory of CITEPA).

Study	Station	Catchment area	Years	CH_4 $t(CH_4)\,km^{-2}\,yr^{-1}$	N_2O $kg(N_2O)\,km^{-2}\,yr^{-1}$
This study	Puy de Dôme (night)	Auvergne region	2010–2012	6.2±3.5	1546±912
CITEPA (2010)	Emission inventory	Auvergne region	2007	6.0±3.0	320±640
Biraud et al. (2000)	Mace Head	Western Europe	1996–1997	4.8–3.5±1.5	475–330±120
Schmidt et al. (2001)	Schauinsland	Western Europe	1996–1998		1180±345
van der Laan et al. (2009a)	Lutjewad	the Netherlands	2006–2009	15.2±5.3	900±300
Lopez et al. (2012)	Trainou (180 m a.g.l.)	Central region (France)	2009–2012		520±156

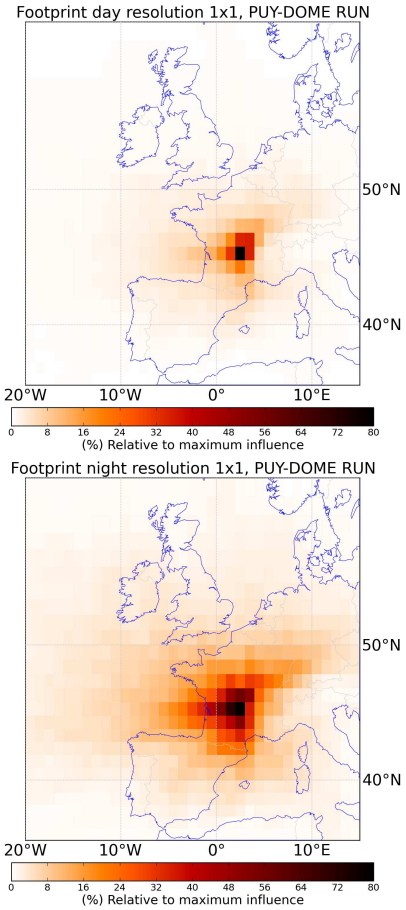

Figure 1. Footprint of the Puy de Dôme station from the Lagrangian dispersion model Flexpart **(a)** during daytime (14:00 to 16:00 UTC), when the PBL is usually well developed, and **(b)** during nighttime (22:00 to 06:00 UTC), when the station is usually in the free troposphere.

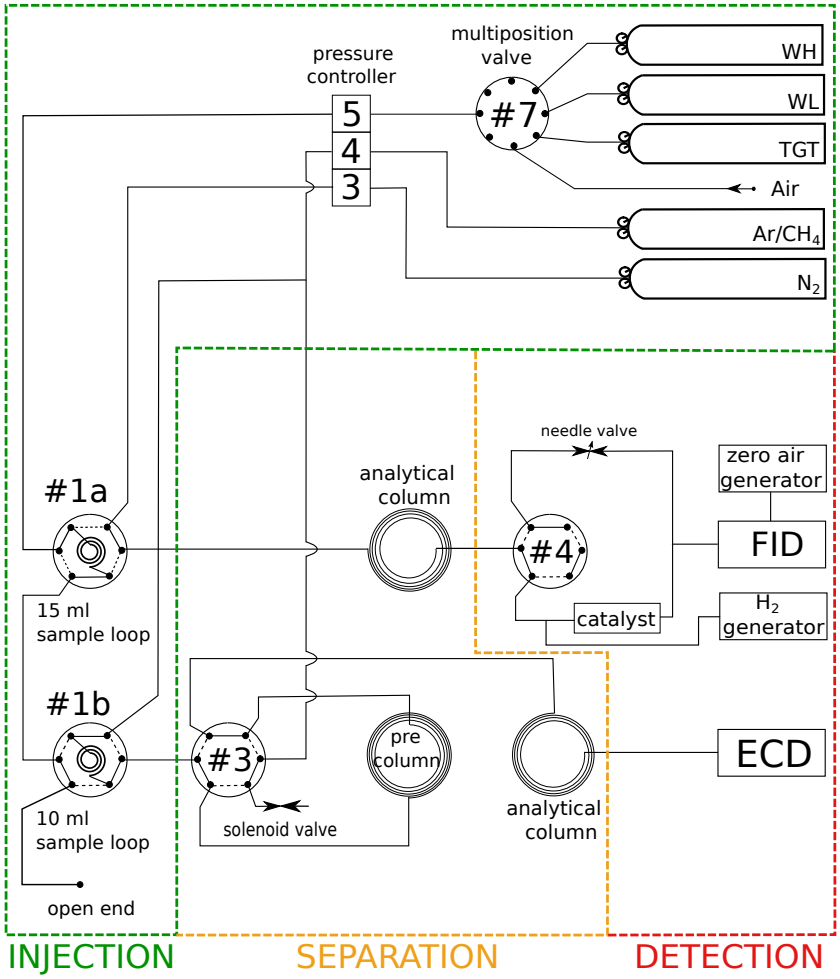

Figure 2. Schematic of the GC system setup (gas flow) at the Puy de Dôme station.

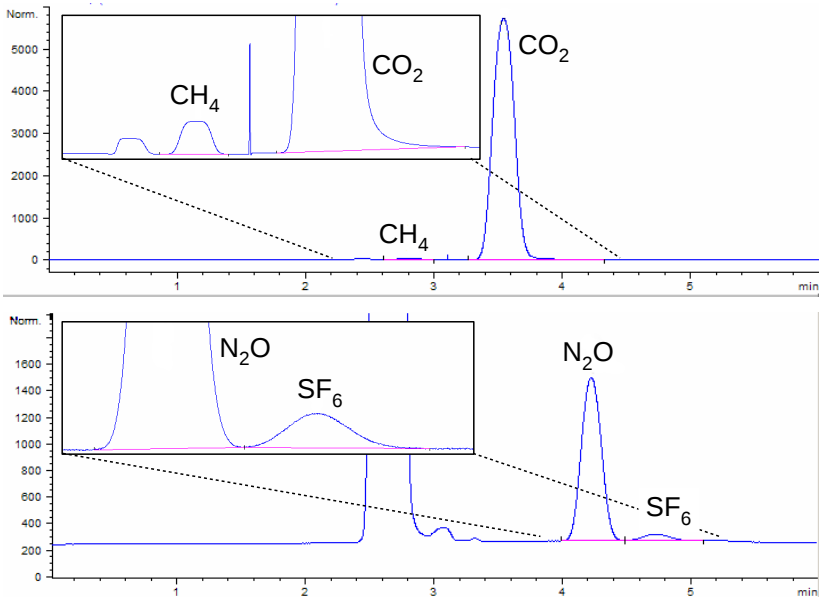

Figure 3. Typical chromatograms obtain on the FID (top panel) and on the μECD (bottom panel).

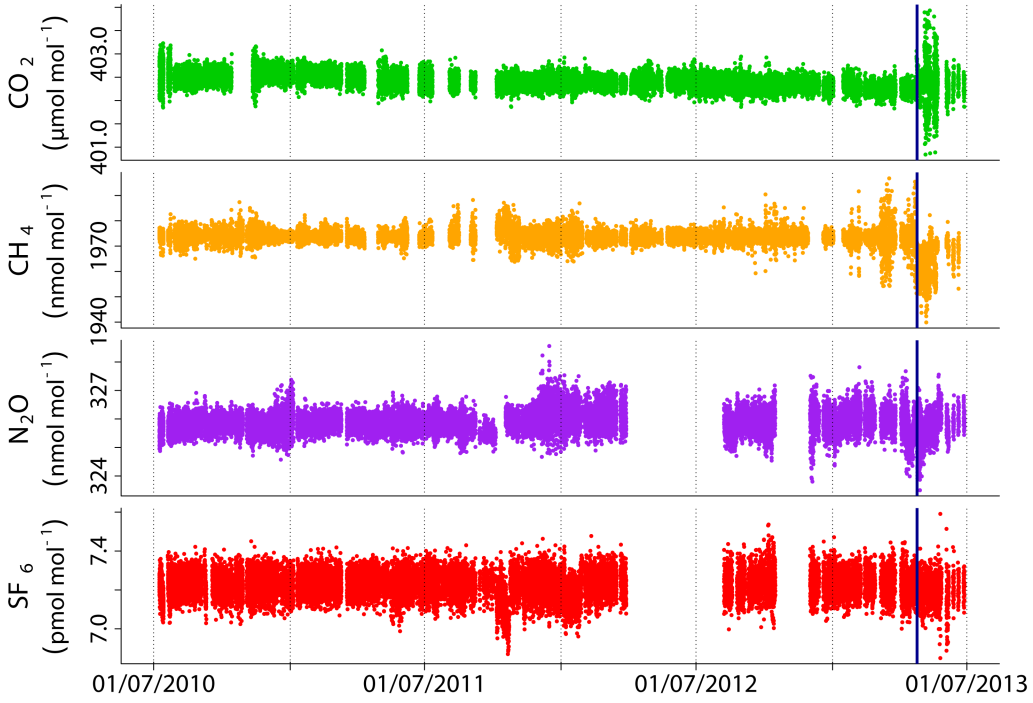

Figure 4. Time series of the target gas measured with the GC system at Puy de Dôme. The vertical blue lines on each panel correspond to the date of the working standards change.

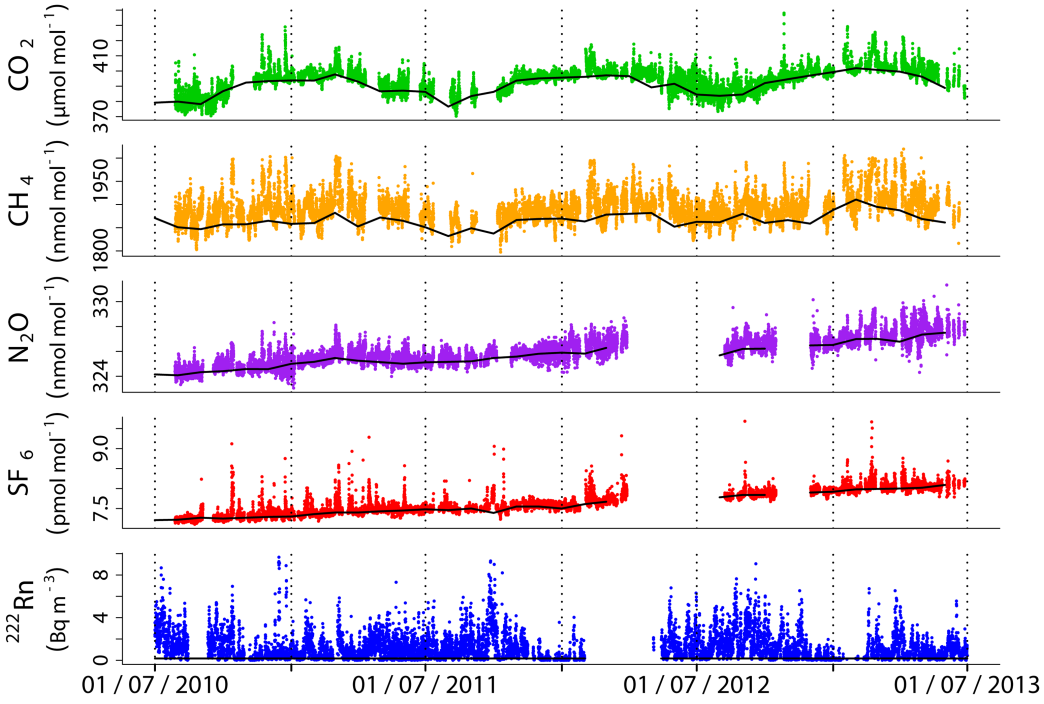

Figure 5. Hourly mole fractions of CO_2, CH_4, N_2O and SF_6 atmospheric ambient air and hourly activities of ^{222}Rn at Puy de Dôme from July 2010 to June 2013. The black lines are the respective monthly GHG background mole fractions of the Puy de Dôme measurements (between 22:00 and 06:00 UTC) and the ^{222}Rn background activity at Mace Head (Ireland).

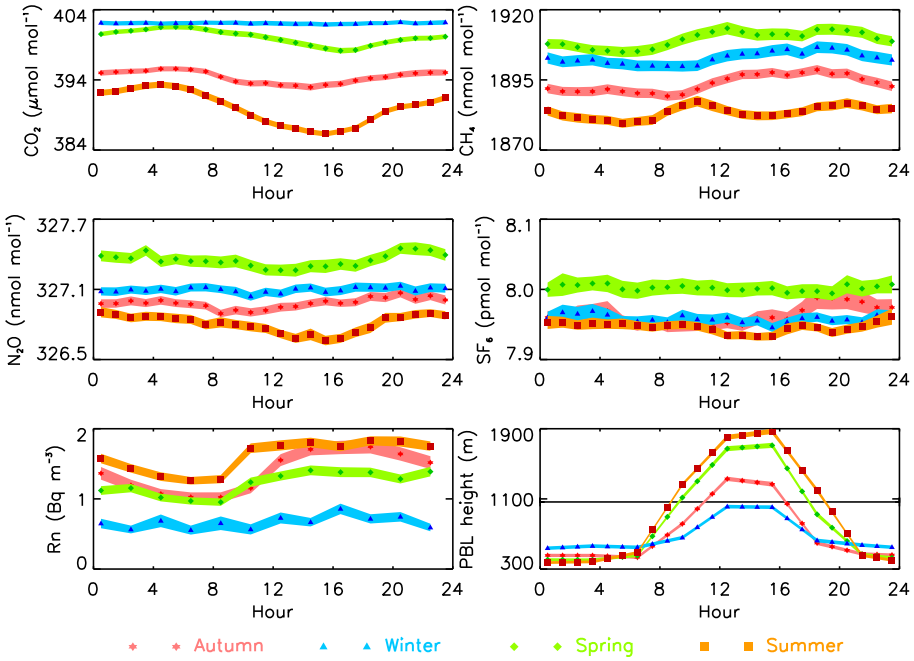

Figure 6. Mean diurnal cycles of CO_2, CH_4, N_2O, SF_6, and ^{222}Rn together with the planetary boundary layer height (relative to Clermont-Ferrand altitude – 396 m a.s.l.) at the Puy de Dôme station for each season. Trace gas mole fractions were detrended based on 1 January 2013.

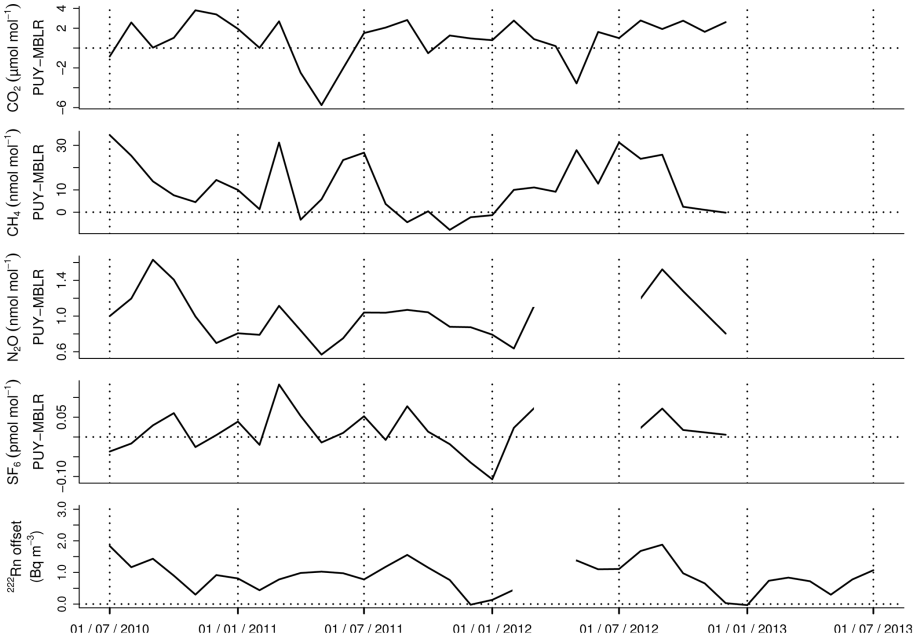

Figure 7. Differences between the monthly background at Puy de Dôme and the respective monthly MBLR (Dlugokencky et al., 2013b, a) at 45.5° N latitude for CO_2, CH_4, N_2O and SF_6. The last panel is the ^{222}Rn offset relative to marine air.

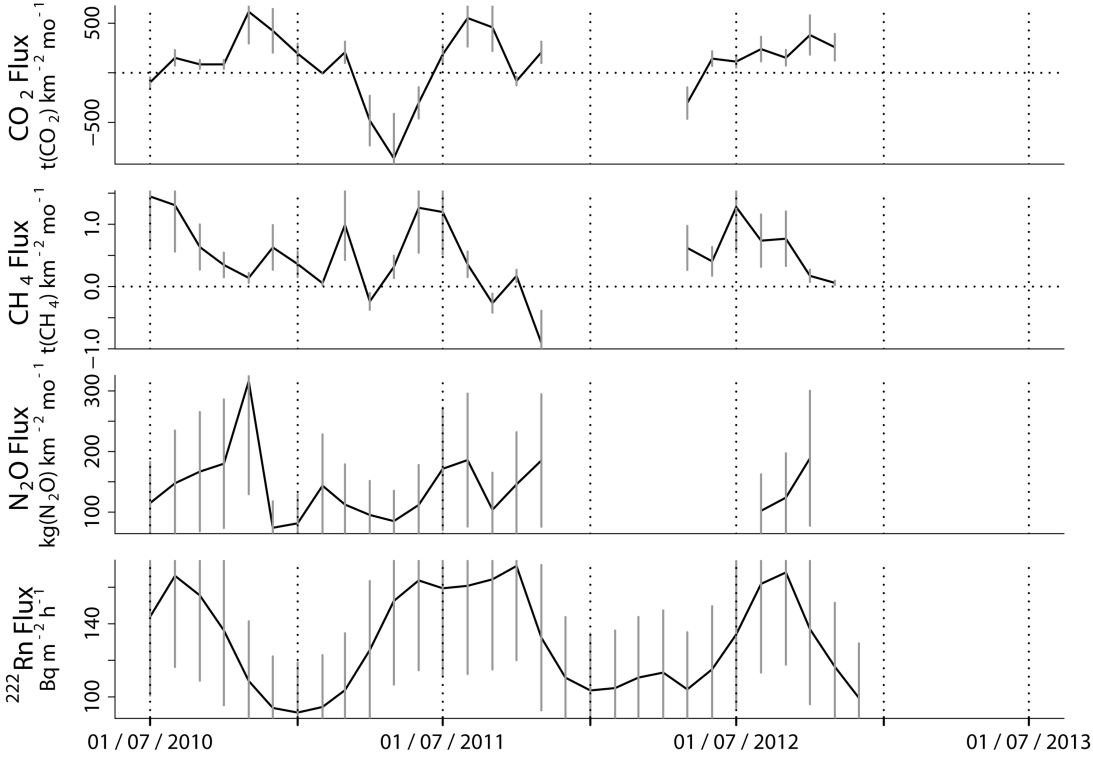

Figure 8. Monthly CO_2, CH_4 and N_2O fluxes at the Puy de Dôme station derived from the radon tracer method. The last panel presents the hourly ^{222}Rn exhalation rate (U. Karstens and I. Levin, personal communication, 2014). The vertical grey lines are the respective flux uncertainties.